Authors' accepted manuscript
Article published in Construction and Building Materials, Vol. 281, 2021.
The final published version available at https://doi.org/10.1016/j.conbuildmat.2021.122568

The effect of air-entraining admixture and superabsorbent polymer on bond behaviour of steel rebar in pre-cracked and self-healed concrete

Seyed Sina Mousavi [1]*, Lotfi Guizani [2], Chandrasekhar Bhojaraju [3], and Claudiane Ouellet-Plamondon [4]

Abstract

This paper intends to study the effect of air-entraining admixture (AE) on self-healing method at rebar-concrete interface using superabsorbent polymer (SAP). AE with a constant dosage of 0.83 kg/m^3, and 0.25% and 1.0% SAP dosages are considered. Two types of superabsorbent polymer with different chemical compositions and particle sizes are considered for the experimental tests. Pull-out test results of mixtures containing AE admixture are compared with those in non-AE concrete. Scanning electron microscopy/energy dispersive X-ray spectrometry (SEM/EDS) along with microscopic analysis is performed to study the healing products at crack surface and SAP macro voids around the rebar.. Overall, results indicate that AE admixture has a considerable impact on the performance of the self-healing method at the rebar-concrete interface especially for higher dosage of SAP (1.0%). This can be attributed to the internal voids networks around the

[1] PhD Candidate, Department of Construction Engineering, École de Technologie Supérieure, 1100 Notre-Dame West, Montreal, Quebec, Canada H3C 1K3 (corresponding author), Email: seyedsina.m@gmail.com, seyed-sina.mousavi-ojarestaghi.1@ens.etsmtl.ca
[2] Associate Professor, Department of Construction Engineering, École de Technologie Supérieure, 1100 Notre-Dame West, Montreal, Quebec, Canada H3C 1K3, Email: lotfi.guizani@etsmtl.ca
[3] Associate Professor, St Joseph Engineering College, Vamanjoor, Mangaluru 575028, Karnataka, India, Email: chandrasekhar.b@sjec.ac.in
[4] Associate Professor, Department of Construction Engineering, École de Technologie Supérieure, 1100 Notre-Dame West, Montreal, Quebec, Canada H3C 1K3, Email: claudiane.ouellet-plamondon@etsmtl.ca

rebar generated by AE admixture, which can ease the water transfer between SAP macro voids to participate in healing cracks after wet-dry cycles. SEM analysis shows that stalactites, healing products at the external surface of crack, are composed of a large amount of calcium and oxygen.

Keywords*:* bond behaviour; air-entraining admixture; superabsorbent polymer; self-healing; pre-cracking phenomenon

1 Introduction

The interaction between reinforcing bar (rebar) and surrounding concrete, known as the "bond-slip" phenomenon, plays a crucial role in the structural behaviour of a reinforced concrete (RC) member. The bond-slip phenomenon affects the structural efficiency of different sub-elements in an RC frame including column [1, 2], beam [3], interior and exterior beam-column joint [4, 5], and slab [6, 7]. Improving bond characteristics can considerably affect the structural performance of these sub-elements along with the integrity of RC frame. Previous studies have shown that concrete composition has a considerable influence on bond properties including water-to-cement ratio [8, 9], mineral admixture [10, 11], aggregate type [12, 13], and chemical admixture [14]. Among these variables, there is no specific study on the effect of air-entraining (AE) admixtures on bond characteristics of steel rebar in uncracked and pre-cracked specimens.

Air-entraining (AE) admixtures are organic surfactants which entrain a controlled quantity of air in concrete that is a uniformly dispersed discrete bubbles [15]. Content, size, spacing and specific surface of air voids are important parameters for AE concrete mixture. Regarding the size distribution of air voids, a wide range of values for different types of AE admixtures was obtained by previous studies. For instance, air void sizes with ranges of 0.25-1.0 mm [16], 0.10-2.0 mm [17], and air voids with a diameter larger than 0.1 mm (without specifying the max diameter) [18] were reported by the literature for AE concrete mixtures. Initial water-to-cement ratio, type of AE admixture, and dosage of AE admixture considerably affect the size distribution of the air-void system [19]. AE admixtures, as a surfactant, reduce the surface tension of water, resulting in bubble formation and stabilization [20]. Uniform dispersion and appropriate stability are obtained by the mutual repulsion of the negatively charged air-entrainer molecules and the attraction of the air-entrainer molecules for the positive charges on the cement particles [21]. AE increases the workability and consistency of concrete [22-24], so that mixtures with AE admixture have a higher slump value as compared to normal concrete (NC) at the same water content. On the other hand, the presence of air bubbles acts as a lubricant. AE concrete is less sensitive to bleeding and segregation than is non-AE concrete [15]. AE admixtures have no noticeable impact on the hydration rate of cement or on the heat evolved by that process. The strength of the hardened concrete is decreased as the amount of air is increased.

Most of the previous studies on the field of AE concrete concentrated on the resistance of mixtures exposed to low temperatures (winter exposure) and freeze-thaw cycles in water-saturated RC members such as outdoor slabs, pavements and bridges [25, 26], i.e., durability problem in cold climates. Perenchio et al. (1990) [27] postulated that the diffusion of gel water to capillary pores encompassing ice causes the growth and expansion of ice lenses, results in generating micro cracks. The freezing cycle increases the width of these micro-cracks, which afterward filled with water during thawing cycles. This cycle causes a rapid deterioration of concrete. Frost damage of concrete can be attributed to the osmotic pressure, in which unfrozen water is compelled to capillary pores under a salt concentration gradient [28]. The growth of ice in such locations causes considerable degradation. The resistance of hardened concrete to this type of damage is considerably improved by the use of AE admixtures [20, 29-33]. This is achieved by the presence of stabilized entrained-air bubbles network within concrete mixture generated by AE admixture, acting as expansion chambers to accommodate the ice formed within the capillaries [34, 35]. Moreover, for a given workability, AE concrete is more durable, as compared to the non-AE concrete by providing lower water-to-cement ratio [36]. Total volume of the entrained air, average volumic surface, and spacing of the air bubbles are the fundamental characteristics of this "air bubble network", which is comprehensively discussed by Gagné (2016) [37]. These air bubbles need to be homogeneously dispersed in the mix, which can be characterized by what is called the "spacing factor of the bubbles network".

Despite the extensive studies on the effect of stabilized air bubble network (provided by AE admixture) on durability properties of concrete, there is no specific study to determine the effect of AE admixture on bond properties of steel rebar embedded in intact and internally-damaged concrete specimens. Moreover, there is no study so far demonstrating the effect of AE admixture on the autogenous healing capacity of concrete with or without healing agents at the rebar-concrete interface. Hence, the present study intends to fill these research gaps by using AE admixture within the mixtures to partly or entirely mitigate internal damages, due to the pre-cracking phenomenon, at the rebar-concrete interface using the self-healing method. Superabsorbent polymer (SAP) is used in the present study to accelerate the self-healing capacity of concrete. Regarding SAP, most of the previous researches only concentrated on autogenous shrinkage [38, 39], drying shrinkage [38], fresh properties and passing ability [40], tensile strength [41], compressive strength [40, 42, 43], chloride ion permeability [39], and self-sealing and –healing cracks [44-46]. However, only NC was studied in the literature. Moreover, only a few studies focused on the self-healing method by SAP to mitigate internal damages at the rebar-concrete interface [47, 48]. Additionally, although there is a growing tendency to study the pre-cracking phenomenon in steel-congested regions such as beam-column joints and shear walls [49-51], only NC was considered by the literature. Hence, to extend the previous study for the cold regions, where using AE admixture is necessary, the main objectives of the present study are as follows:

1- How much does the AE admixture affect the bond strength of steel rebar in pre-cracked concrete?

2- How much AE admixture is efficient for the self-healing method by SAP at the steel rebar-concrete interface?

To address these questions, an extensive experimental plan is conducted in the present study. Results are comprehensively compared with the results of a recently published paper by authors for NC [47]. Three main statuses of specimens are used including uncracked, pre-cracked, and healed specimens. Statistical analysis is also carried out, to identify the most significant factors affecting performance of the self-healing method.

2 Experimental program

2.1 Material properties and experimental plan

Five concrete mixtures are considered for this study to compare the results between AE concrete with non-AE concrete (reported by recently published paper by authors [47]). Mixtures were designed to determine the effect of different parameters including (a) SAP percentages; (b) SAP size and chemistry; (c) concrete flowability; and (d) AE admixture on bond behaviour of uncracked, pre-cracked, and healed specimens. The concrete composition of AE mixtures is illustrated in Table 1. Details of non-AE mixtures for both NC and SAP-modified NC were mentioned in Mousavi et al. (2020) [47]. General use (GU) cement was used for all mixtures with a density of 3.15 g/cm^3. Natural sand with a maximum grain size of 1.25 mm and a specific gravity of 2.68, and gravel with a nominal maximum diameter of 14 mm and a particular gravity of 2.68 were considered for mixtures. The SAP was added at a range of 0.0-1.0 wt.% of cement for non-AE concrete and only 0.25% and 1.0% for AE-contained mixtures. To adjust the flowability of concrete mixtures, superplasticizer was added, at different proportions. AE concrete mixtures contained an aqueous solution compound of synthetic chemicals by 0.83 kg/m^3 of concrete mixture, with a specific gravity of 1.006, 7.5% of solids by weight, and a pH of 11.0.

Two different types of SAP were considered in this experimental study including (1) SAP-1, a cross-linked copolymer of acrylamide and potassium acrylate with a maximum particle size of 500 µm. SAP-1 had water absorption of 249 g/g (gram water per gram of SAP) and 25 g/g in deionized water and pore solution, respectively; (2) SAP-2, a crosslinked anionic polyacrylamide with a maximum particle size of 150 µm. SAP-2 had water absorption of 170 g/g and 25 g/g in deionized water and pore solution, respectively. The water absorption capacity of SAPs was measured by three different methods [47] including (1) the tea bag method; (2) the slump test method; and (3) the water desorption method (the absorption of a centrifuged cement pore solution). Both SAP types were produced through the bulk polymerization method, where blocks of polymers were powdered into irregular-shaped powder [47]. The specific values d10, d50, and d90 correspond to sphere diameters that have volumes equal or larger than 10 vol%, 50 vol%, and 90 vol% of the total volume of the particles, respectively. The median particle size (d50) of dry SAP particles were 260 µm and 47 µm for SAP-1 and SAP-2, respectively. The small diameters (d10) of dry SAP particles were 92 µm and 13 µm for SAP-1 and SAP-2, respectively. The large diameters (d90) of dry SAP particles were 450 µm and 92 µm for SAP-1 and SAP-2, respectively. Specific gravity values of SAP-1 and SAP-2 are 1.51 and 1.49, respectively. Bulk densities of SAP-1 and

SAP-2 were 0.82 and 0.84, respectively. Specimens were initially cured 28 days in the moisture room at 97.3% RH and 23 ºC. Those healed specimens, which were subjected to wet-dry healing cycles, kept in the curing tank for longer periods of 14 and 28 days (20 ºC, 60% RH) after pre-cracking. One wet-dry healing cycle represents 24 hours in water followed by 24 hours in dry condition (normal atmospheric or laboratory-controlled conditions). Consequently, 7 and 14 cycles took 14- and 28-day wet-dry healing cycles, respectively. Configurations of concrete mixtures studied in the present study are illustrated in Table 2. Reference mixes were designated by "R", "RA-1", and "RA-2". Character "A" in the names of some mixtures determines AE mixtures. "S1" and "S2" correspond to mixtures containing SAP-1 and SAP-2 respectively. Numbers of 25, 50, and 100 in some mixtures show 0.25%, 0.50%, and 1.0% SAP by weight of cement respectively. Cylindrical specimens with diameter of 150 mm and height of 113 mm were considered for pull-out specimens. Embedded length was $5d_b$ for all specimens. Steel rebar with nominal diameter of 10 mm, rib spacing of 13.22 mm, and rib height of 1.89 mm was used in the experimental specimens. Specified yield strength and ultimate tensile strength of steel rebar were 432 MPa and 620 MPa, respectively. Three repetitions were considered for uncracked specimens. However, due to the brittle nature of splitting tests (to simulate the pre-cracking phenomenon), specimens with different crack widths were obtained so that less than 3 specimens were tested for some pre-cracked and healed specimens. The designation of specimens is as follows: first character in specimen identification describes mixture type including R=reference; RA2=reference mix with AE admixture; 25S1=0.25% SAP-1; 25S2=0.25% SAP-2; 50S1=0.5% SAP-1; 100S1=1.0% SAP-1; 25S1A=0.25% SAP-1 with AE admixture; 25S2A=0.25% SAP-2 with AE admixture; and 100S1A=1.0% SAP-1 with AE admixture. The second character indicates the initial crack width before healing; For instance, C0.3= crack width of 0.30 mm. The last character determines the healing period so that 14H and 28H show specimens after 14- and 28-day healing periods, respectively.

2.2 Experimental procedure

The pre-cracking test was carried out as detailed in Mousavi et al. (2019 & 2020) [47, 49, 50]. Controlled Brazilian tests (splitting), recommended by Desnerck et al. (2015) [52], were used to produce different crack widths parallel to the rebar direction (Fig. 1(a)). To control crack opening, crack gauges were installed at both sides of specimens, along with a manual measurement of crack widths. Based on empirical observations, the displacement rate of 0.11-0.15 mm/min was considered for splitting tests. Crack widths ranging from 0.10 to 0.50 mm were obtained by the splitting tests. Then, direct pull-out tests were conducted after three stages of uncracked, pre-cracked (by a splitting test), and healed (after 14 and 28 days re-curing) specimens with a displacement rate of 0.50 mm/min (Fig. 1(b)). Slip was measured at the free-end of the steel rebar during the pull-out test. To prevent corrosion influences for 28-day healing periods, the heat-shrinkable tube was used at both end sides of specimens (Fig. 1(c)). To analyse the results, maximum bond stress (or bond strength, τ_u), residual bond stress which corresponds to the bond stress value observed at an almost constant plateau, following the descending branch of the bond-slip curve and starting at a slip of 10 mm (τ_r), and area under the bond-slip curve until the slip of 12 mm (absorbed energy) are used in the present study. Moreover, as recommended by RILEM [53], average bond stress (τ_m) is used as the arithmetic mean of bond stresses of $\tau_{0.01}$, $\tau_{0.1}$, and $\tau_{1.0}$ corresponding to slips of 0.01 mm, 0.10 mm, 1.0 mm, respectively.

2.3 Experimental results

Three main characteristics of average bond stress (τ_m), maximum bond stress called bond strength (τ_u), and residual bond stress (τ_r) are considered in the following subsections to analyse the results. General observations showed that uncracked and cracked specimens with $w < 0.15$ mm experience pulling out the rebar from the concrete cylinder without noticeable propagation of splitting cracks (perpendicular to the rebar) (Fig. 2(a)). This corresponds to the high value of concrete cover-to-rebar diameter ratio, providing enough confinement surrounding the rebar in uncracked specimens to completely shear-off concrete key between two adjacent ribs. However, $w > 0.15$ mm leads to complete splitting of the specimens and slippage out of the rebar (Fig. 2(b)). Large initial cracks cause rebar-concrete surface separation and a considerable reduction in concrete confinement surrounding the rebar. As explained in literature [50], this surface separation due to the pre-cracking phenomenon change the failure mode from pull-out (shear-off concrete key) to crushing a wedge-shaped concrete block on the rib front face (splitting failure mode). Similar observations were obtained for failure modes of healed specimens so that splitting failure modes were observed for partly and fully recovered bond strength specimens. Results show that the accelerated self-healing method by SAP cannot improve the failure mode after healing periods. Compressive strength of concrete mixtures is shown in Fig. 3. Generally, results indicate that 25S1A is the optimum mixture among other air-entrained mixtures. Results show that using AE causes considerable reduction effect on the compressive strength so that strength reductions of 18.6%, 7.0%, 16.5%, and 33.2% are obtained for mixtures of RA-1, 25S1A, 25S2A, and 100S1A repectively (Fig. 3(a)). Moreover, results show that AE has lower impact on the compressive strength of concrete containing SAP with larger particle size (25S1A) as compared to the smaller size SAP (25S2A). Besides, results show that AE has higher devastating impact on the compressive strength of mixture contaning higher dosage of SAP (100S1A) as compared to the lower dosage (25S1A). As illustrated in Fig. 3(b), the present study proposes Eqs. (1) and (2) for the 28 days compressive strength of non-air-entraining and air-entraining SAP concrete mixtures respectively, as a function of the totall water-to-cement ratio (W_T/c), as follows:

$$f'_c = 152.7e^{-2.31(W_T/c)} \tag{1}$$

$$f'_c = 163.62e^{-3.0(W_T/c)} \tag{2}$$

2.3.1 Uncracked concrete

Results of uncracked concrete are shown in Fig. 4 for all mixtures. To compare all mixtures, the effect of concrete compressive strength is eliminated by normalization. This is achieved by dividing these stresses by the square root of the concrete compressive strength including normalized average bond stress, ${\tau_m}^* = \tau_m/\sqrt{f'_c}$, normalized bond strength, ${\tau_u}^* = \tau_u/\sqrt{f'_c}$, and normalized residual bond stress, ${\tau_r}^* = \tau_r/\sqrt{f'_c}$. Results indicate that RA-2 and R mixtures have the highest normalized average bond stress among other mixtures (Fig. 4(a)). In the case of normalized bond strength, RA-2 has higher values (4.2), as compared to other mixtures (Fig. 4(b)). Similar results are observed for normalized residual bond stress (Fig. 4(c)) and energy dissipated by the bond mechanism (Fig. 4(d)). This can be attributed to the higher slump value of RA-2, which affects the rebar-concrete bond strength. Generally, results indicate that concrete composition has a significant impact on bond properties of steel rebar embedded in uncracked concrete specimen, which was similarly confirmed by the literature [10, 54-56]. Only lightweight aggregate concrete (LWC) was considered in concrete design codes due to a lower bond strength of steel rebar in LWC as compared to NC, while results of the present study emphasize that specific specifications are required for different concrete mixtures.

2.3.1.1 Effect of SAP percentage on bond strength of AE and non-AE concrete

Fig. 5 shows the effect of SAP percentage on the bond response of uncracked specimens. General results show that SAP percentage higher than 0.25% leads to a significant reduction in the normalized bond properties in uncracked specimens due to the higher number of SAP macro pores around the rebar. In the case of low dosage of SAP (0.25%), 2.9% and 0.0% bond strength reductions are obtained for AE and non-AE concrete mixtures, respectively. As mentioned in literature, this slightly bond strength reduction of a low dosage of SAP can be compensated by using fiber within the mixture to control the crack width [57, 58]. In the case of non-AE concrete, general results show that a higher dosage of SAP causes a considerable reduction in bond properties, especially for the residual bond stress (Fig. 5(a)). Among the bond properties, SAP dosage has higher effect on the maximum bond strength (44.1%), while lower impact on the residual bond stress (77.8%) for non-AE concrete. However, different trends are followed by AE concrete, so that approximate reduction of 50.0% is observed for all bond properties of 100S1A mixture (Fig. 5(b)). In the case of 0.25S1A mixture, 4.8% and 10% increases were recorded for the average and residual bond stress, respectively. This finding can confirm the fact that AE admixture is in good combination with 0.25% SAP for using in concrete mixtures. Despite the findings of the present section, more experimental studies are necessary for future works to confirm the obtained results.

2.3.1.2 Effect of AE admixture on bond strength of AE and non-AE concrete

In the case of reference mixture (R), AE admixture has no considerable effects on the maximum and average bond stress (Fig. 6(a)), while 44.0% reduction is obtained for the residual bond stress. For 0.25% SAP-1, maximum and residual bond stresses are the same for both AE and non-AE mixtures, while the average bond stress of 25S1A mixture is 29.0% more than that of 25S1 mixture (Fig. 6(b)). Similar results are obtained for 1.0% SAP-1 (Fig. 6(d)). However, results show that AE admixture has negative impacts on bond properties of SAP-2, so that 22.0%, 30.0%, and 62.0% reductions of average bond stress, bond strength, and residual bond stress are obtained respectively for using AE admixture (Fig. 6(c)), which is similar to the trend of the reference mixture (R, Fig. 6(a)). Hence, comparable and higher bond properties of SAP-1 presented in Fig. 5(b), and Fig. 6(b and d) show the fact that SAP-1 is more adaptable with AE admixture when compared with SAP-2.

2.3.1.3 Effect of SAP particle size and type on bond strength of AE and non-AE concrete

The effect of SAP particle size (and/or chemistry) is shown in Fig. 7. Bond properties are normalized by the square root of the concrete compressive strength of mixtures ($\tau/\sqrt{f'_c}$). Results show that in the case of non-AE mixtures, SAP-2 has higher bond properties as compared to SAP-1. However, the results of Figs. 6 and 7 indicate that SAP-1 is more adaptable with AE admixture as compared to SAP-2. This can be attributed to different chemical compositions of SAP used, changing their absorption behaviours including total capacity and sorption kinetics. Moreover, different sizes of these healing agents ($d50_{\mathrm{SAP-1}}$ >> $d50_{\mathrm{SAP-2}}$) can affect the absorption kinetics and microstructure of concrete mixture. Using different types of SAP changes the interfacial transition zone (ITZ) around the rebar, which is different from the effect of SAP on concrete compressive strength [10]. In this context, Mousavi et al. (2020) [52] showed that SAP-2 produces a higher number of pores in paste around the rebar with a smaller void size. Therefore, the porosity pattern of SAP-2-contained concrete is different from SAP-1-contained concrete. A similar trend is reported by the literature [9, 10, 59], where the effects of water-to-cement ratio (w/c) and concrete composition were confirmed at ITZ around the rebar. It is worth mentioning that as the chemical part of SAP used is out of the scope of the present study, more experimental studies are necessary for future works to highlight the obtained results.

2.3.2 Pre-cracked concrete

Results of 100 pre-cracked pull-out specimens (excluding healed specimens) are summarized in Fig. 8 by the normalized reduced bond ratio ($(\tau)_c/(\tau)_{un}$) versus crack width-to-rebar diameter ratio (w/d_b). Parameters of $(\tau)_c$ and $(\tau)_{un}$ corresponding to the bond properties of cracked and uncracked specimens, respectively. The significant impacts of the pre-cracking phenomenon on the average bond stress, bond strength, and residual bond stress are clear. Results show that residual bond stress is considerably affected by the initial induced cracks, so that even small crack widths cause more than 50.0% reduction in bond strength. However, three out of trend data is recorded for the residual bond stress with $\tau_c > \tau_u$. The following equations are proposed for reduced bond ratio after induced crack width:

$$\left(\frac{(\tau)_c}{(\tau)_{un}}\right)_m = 352.3\left(\frac{w}{d_b}\right)^2 - 36.4\frac{w}{d_b} + 1.0 \qquad (3)$$

$$\left(\frac{(\tau)_c}{(\tau)_{un}}\right)_u = 26160.4\left(\frac{w}{d_b}\right)^3 - 1609.2\left(\frac{w}{d_b}\right)^2 + 1.67\frac{w}{d_b} + 1.0 \quad (4)$$

$$\left(\frac{(\tau)_c}{(\tau)_{un}}\right)_r = 533.74\left(\frac{w}{d_b}\right)^2 - 46.5\frac{w}{d_b} + 1.0 \quad (5)$$

For uncracked specimens ($w = 0$), proposed equations are equal to one, showing $(\tau)_c = (\tau)_{un}$. These equations are obtained for $0 < w/d_b < 0.05$. Moreover, only nominal $d_b = 10$ mm rebar is used to normalize the initial crack width. So, more experimental studies with different values of w/d_b are necessary to be performed by future studies to confirm the proposed trend. To determine the effect of AE on the pre-cracking phenomenon, the results presented in Fig. 8 is divided in two separate groups of mixtures with AE and mixtures without AE for the average bond stress, the bond strength, and the residual bond stress (Fig. 9). Overall, trends obtained for AE-contained mixtures show that AE causes a higher bond reduction factor, leading to being less sensitive to the internal damages due to the pre-cracking phenomenon (Fig. 9(a)). Similar results are obtained for the bond strength and the residual bond stress (Figs. 9(b) and (c)). As crack width increases, this deviation increases. Generally, results indicate that concrete composition has a significant impact on bond properties of steel rebar embedded in pre-cracked concrete, which was similarly confirmed by previous studies [47, 54]. Proposed equations for predicting bond reduction factors are illustrated in Fig. 9. The effect of AE admixture on the pre-cracking phenomenon (i.e. bond properties) is illustrated in Figs. 10, 11, and 12 for the average bond stress, the bond strength, and the residual bond stress, respectively. General results of bond properties reduction show that concrete mixtures containing AE admixture are less sensitive to the pre-cracking phenomenon (higher $(\tau)_c/(\tau)_{un}$ ratio), as compared to the non-AE concrete mixtures. This may be attributed to the high flowability (slump flow) of AE mixtures, which is shown in Table 2. Similar observation was confirmed by literature [54], where SCC mixtures showed less sensitivity to the pre-cracking phenomenon as compared to NC.

2.3.3 Healed concrete

An improvement factor (IF) is defined in this section by Eq. (6) to measure the performance of SAP and AE for healing cracks at the rebar-concrete interface in different mixtures. As IF increases, the healing efficiency of the mixture increases. Zero value of IF corresponds to the specimens with lower or comparable bond properties than the cracked specimen with constant crack width ($\tau_{Healed} \leq \tau_{Precracked}$), while $IF > 0$ represents the healed specimens with higher bond properties as compared to those of pre-cracked specimens ($\tau_{Healed} > \tau_{Precracked}$). It is necessary to emphasize that due to the brittle nature of concrete in tension, different crack widths were obtained by splitting tests. Hence, to compare bond results of healed specimens with cracked ones, bond reduction-crack width curves were used to predict bond properties of cracked specimens, in the case that different cracks were generated.

$$IF = \left[\frac{\tau_{Healed} - \tau_{Precracked}}{\tau_{Uncracked} - \tau_{Precracked}}\right] \times 100 \qquad (6)$$

A total number of 63 healed specimens for 14- and 28-day healing periods (in water tank) were tested in the present study. Improvement factor for the average bond stress (IF_{τ_m}) with a determined standard deviation (SD) is illustrated in Fig. 13 for all mixtures. Considerable healing of 0.15 mm crack widths after 28-day healing periods by 100S1A mixture is clearly depicted in Fig. 13, which is higher than 100% (IF_r=152.6%). However, a high SD is obtained for this case.

In this field, the reference mixture improved the average bond stress (τ_m) by 22.0% and 8.4% for crack widths of 0.30 mm and 0.40 mm, respectively. Moreover, mixtures of 25S1, 50S1, 100S1, 25S1A, and 25S2A improved self-healing capacity up to $IF_{\tau_m} \leq 25.4\%$ for average bond stress. Results of bond strength are more important as compared to other results, as this parameter affects directly structural and anchorage capacity. Similar to the average bond stress, concrete mixtures containing 1.0% SAP (100S1A and 100S1A) have significant improvement factor of bond strength (Fig. 14). General results of IF_{τ_u} indicate that a reference mixture without a healing agent has a low improvement factor (5.7%), as compared to SAP mixtures. In this field, mixtures of 25S1, 50S1, 25S1A, and 25S2A show $IF_{\tau_u} \leq 58.0\%$. It is clearly observed that SAP has a real potential of self-healing capacity and mitigating damage due to the pre-cracking phenomenon at the rebar-concrete interface. Similar results of the residual bond stress healing (IF_{τ_r}) are obtained for mixtures of 50S1, 100S1, and 100S1A (Fig. 15). Compared to the bond strength and the average bond stress, a lower improvement factor is observed for the residual bond stress of other mixtures. The general trend observed in Figs. 13-15 shows that SAP has considerable influences on healing cracks for mitigating damages, especially for mixtures of 50S1, 100S1, and 100S1A.

Bond-slip curves of 100S1A mixtures are illustrated in Fig. 16 for the pre-cracked and the healed specimens. Due to the low tensile strength of mixtures containing 1.0% SAP and AE, crack width of 0.15 mm is considered in the splitting test for this type of mixture. Pull-out failure modes are observed for this small crack width, which is obvious from the bond-slip curves, where no sudden drop presence after the maximum bond stress (Fig. 16(a)). Results show that the bond strength is considerably increased after both 14- and 28-day healing periods (Fig. 16(b)). Moreover, slip corresponds to the maximum bond stress is also increased along with strength recovery. Initial ascending parts of the bond-slip curve for different specimens are shown in Fig. 16(c). Results show that the healed specimens have higher initial stiffness as compared to the cracked specimens. A similar observation is achieved for the residual bond stress (Fig. 16(d)). Energy absorbed (dissipated) by bond mechanism is also measured by the area under the bond-slip curve up to the slip of 10 mm, which is illustrated in Fig. 16(e). Results show that the self-healing method by 1.0% SAP significantly increased the absorbed energy, as compared to the cracked specimens. Overall, results show that a crack width of 0.15 mm can be mostly recovered by 1.0% SAP and AE.

Bond-slip curves of 25S1A mixtures are illustrated in Fig. 17 for pre-cracked and healed specimens. Crack widths of 0.20, 0.25, and 0.30 mm are generated in the splitting test for this type of mixture. Splitting failure modes are observed for these crack widths. Sudden drops in the bond-slip curves are obtained for cracked specimens (Fig. 17(a)). Scattering results are obtained for this type of mixture with a low dosage of 0.25% SAP. Results clearly show that the 14-day healing period is not enough to recover bond properties. As shown in Fig. 17(b), higher bond strength is obtained for the healed specimens with crack widths of 0.30 mm after 28-day healing periods. Healed specimens have higher initial stiffness of bond-slip curves, as compared with cracked specimens (Fig. 17(c)). However, there are no promising results for residual bond stress of mixtures containing 0.25% SAP with AE (Fig. 17(d)), which is different from 1.0%SAP mixtures (Fig. 17(d). Absorbed energy (dissipated) by the bond mechanism in 25S1A mixture is significantly affected b 28-day healing periods so that even higher area is observed as compared with uncracked specimens (Fig. 17(e)). However, splitting failure modes are observed for all healed specimens. Overall, results indicate that healing specimens cannot change the failure mode.

Bond-slip curves of 25S2A mixtures are illustrated in Fig. 18 for pre-cracked and healed specimens. Crack widths of 0.20-0.40 mm are generated in the splitting test for this type of mixture. Splitting failure modes are observed for these crack widths. Sudden drops in the bond-slip curves are observed for cracked specimens (Fig. 18(a)). For crack width of 0.30 mm, results for 28-day healing periods show higher bond strength as compared to the cracked specimens (Fig. 18(b)). Also, two cracked specimens with $w = 0.40$ mm are considered for 28-day healing periods. General results of the initial stiffness (slop) of bond-slip curve show that healed specimens have slightly higher slop as compared to the cracked specimens, while the trend is weaker for 0.25% SAP (Fig. 18(c)) than 1.0% SAP (Fig. 16(c)). This may be attributed to the small crack width generated (by splitting test) for 1.0% SAP. Similar to 25SAP1A mixture, there is no clear trend for residual bond stress in 25SAP2A mixture. Despite the previous mixture containing SAP and AE, 25SAP2A mixture could not drastically improve the absorbed energy, especially for crack width of 0.25 mm (Fig. 18(e)).

Close photos of the healed specimens are shown in Figs. 19 and 20 (white crystals). Scanning electron microscopy/energy dispersive X-ray spectrometry (SEM/EDS) microanalysis method was conducted to identify and quantify all elements of healed products. A considerable amount of calcium deposits are mostly abundant close and at crack lips, which may be an illustration of calcium carbonate precipitation for healing cracks (Figs. 19 and 20). SEM/EDS results of one sample are illustrated in Fig. 21. To compare the results of SEM/EDS analysis between healing products obtained from the internal and external surfaces of cracks, results of some samples are shown in Fig. 22. Results indicate that healing products at the external surfaces of cracks have a considerably lower content of calcium (Ca), as compared to the internal ones. However, higher content of oxygen (O), carbon (C), and especially magnesium (Mg) are observed for external healing products, as compared to the internal ones. Snoeck et al. (2014) [46] reported that the external healing products consist of $CaCO_3$ and washed out hydration products. However, there is no accurate description of the differences between elements of the internal and the external products.

3 Statistical analysis of healing improvement factor

After presenting the results for non-AE and AE concrete, this section intends to perform a comprehensive statistical analysis to find out (1) the most important parameter affecting the self-healing results; (2) interaction plots of improvement factors with respect to different key variables. To follow this statistical approach, two statistical software of "Minitab" [60] and "STATISTICA" [61] are used. Crack width (w), healing period (H), SAP percentage, SAP type, and AE percentage are the main variables considered for the input of the analysis. Improvement factors of maximum (IF_u), average (IF_m), and residual (IF_r) bond strength are the output results. Additionally, the average values of these three improvement factors (IF_{ave}) is also considered in the analysis. Analysis of variance (ANOVA) is conducted to explain the interaction between variables and also output. The main effects of variables obtained by ANOVA are illustrated in Fig. 23 for the average bond stress, the bond strength, and the residual bond stress improvement factor. Moreover, the average values of theses improvement factors are measured and compared. From the ANOVA analysis on the average improvement factors (IF_{ave}), P-values of 0.015, 0.06, 0.001, 0.91, and 0.12 were obtained for input parameters of crack width (w), healing period (H), SAP percentage ($SAP\%$), SAP type (or size), and AE percentage, respectively. Results indicate that the $SAP\%$ factor is the most influencing factor on the self-healing method, as compared to other parameters, while no clear trend was observed for the SAP type (or size) factor so that high P-alue was obtained for this parameter. Results indicate that crack width smaller than 0.20 mm is fully recovered by wet-dry healing cycles (higher than 50%) (Fig. 23(a)). A similar range of around 0.14 mm is reported by Snoeck et al. (2014) [46] to completely seal cracks by SAP. However, Fig. 23(a) shows that bond strength recovery (crack-healing) is difficult for large crack widths so that IF is around 20% to 25% for $w > 0.20$ mm. Similarly, in this context, Kua et al. (2019) [58] reported that the performance of crack-sealing by the combination of SAP and fiber is low for large crack widths ($w > 0.5\ mm$). It shows that more confinement methods are necessary to limit the initial crack width for improving the self-healing method at the rebar-concrete interface and/or the matrix. Regarding healing periods, ANOVA results show that an average value of 20% is obtained for 14-day wet-dry cycles, while the average value of 35% is obtained for 28-day wet-dry cycles (Fig. 23(b)). As the healing period increases, enough time is available to provide more $CaCO_3$ participation at crack surfaces, which is similarly reported by Snoeck et al. (2018, 2019) [62, 63]. The effect of SAP size (and type) on healing improvement factors is shown in Fig. 23(c). The analysis shows that SAP with larger size (0.50 mm, SAP-1) has considerably higher improvement factor as compared to the smaller SAP (0.15 mm, SAP-2). As comprehensively discussed by Mousavi et al. (2020) [47], concrete containing SAP-1 generates larger macro voids as compared to SAP-2, which may provide more possibility to pass the crack line. However, there is no fact regarding this difference in the literature. Different chemistry types of SAP used may affect the obtained results. The effect of AE admixture on the self-healing capacity of concrete is illustrated in Fig. 23(d). Results show that AE admixture has considerable influences on self-healing capacity so that improvement factor higher than 60% is obtained for the maximum improvement factor of AE mixtures. Fig. 23(e) shows that SAP percentage has considerable influence on improvement factors. Although NC without SAP obtained less than 10% IF, SAP concrete mixtures have a range of $20\% \leq IF < 150\%$ for 1.0% SAP. Average improvement factor (IF_{ave}) has a range 60%-90% for 1.0% SAP percentage. Regarding NC without SAP, IF_u has the lowest value among the improvement factors, while this parameter is increased for 0.25% and 0.50% SAP (Fig. 23(e)). However, in the case of 1.0% SAP which small crack widths are tested, still lower healing capacity is observed as compared to other improvement factors. Moreover, results show that 28-day healing period is enough for regaining residual bond stress, as compared to the bond strength. It seems that more healing periods are necessary to regain bond strength after the pre-cracking phenomenon.

Fig. 24 clearly confirms the results of the previous subsection regarding SAP percentage. Results indicate that a higher dosage of SAP has a significant impact on self-healing capacity, especially after 28-day healing periods and in concrete mixtures containing AE admixture. Based on statistical results obtained in the previous subsections, this section intends to propose a statistical equation to predict average improvement factor (IF_{ave}). A multilinear regression model by STATISTICA software [61] shows that crack width plays a critical role in the self-healing method which has severally confirmed by Snoeck et al. (2014, 2019) [46, 62]. Moreover, SAP% and the healing period have considerable effects on the average improvement factor. However, SAP size has the lowest impact on IF_{ave}, as compared to other variables. Hence, the proposed model ignore this parameter. Finally, the statistical equation of Eq. (7) is obtained to predict average improvement factor (IF_{ave}), as follows:

$$IF_{ave} = -0.30 + 0.18H + 0.46SAP\% + 0.17AE \tag{7}$$

where H is the healing period, $SAP\%$ is polymer percentage replacement by cement weight, and AE is air-entraining admixture percentage replacement by cement weight. Performance of Eq. (7) is shown in Fig. 25. It is worth mentioning that as Eq. (7) was obtained based on the experimental results of the present study, there are always some limitations. For instance, only one healing regime (wet-dry cycle) with limited healing periods (14 and 28 days) was considered. Additionally, one dosage and type of AE was used in the experimental program. Moreover, as emphasized throughout the present study, different SAP types with different chemistries can be used in this context. For aiming that, more experimental studies are necessary for future works to determine the efficiency of the proposed equation.

4 Discussion of the results

As mentioned in the previous sections, SAP percentage, AE, and healing periods have considerable impacts on the crack-healing at the rebar-concrete interface, which is summarized in Eq. (7). This section intends to explain the main reasons for these findings by using the "Buffon needle problem", probability of crack-hitting by SAP particles (Fig. 26). Buffon's problem considers a grid of parallel lines with spacing B and a needle length of D. When the needle is dropped at random, its position and orientation are random [64], the needle intersects at least one line of the grid by the probability of P_T [65]. Regarding SAP-modified concrete, we assume that SAP particles are randomly dispersed in the concrete mixture. As shown in Fig. 26(a), crack pattern is constant in the case of the pre-cracking phenomenon. The process of tossing SAP onto the crack network generates two scenarios including: (1) SAP particles intersecting the cracks; (2) SAP are far from the crack edges. Hence, these scenarios reminds the "Buffon needle problem". For SAP particles, if there are N SAP particles and the crack-hitting probabilities by the SAP (P) are considered the same, the random variable X meaning the total number of intersection in the area, and the mean of X, denoted as $E(X)$, can be given by Lin et al. (2018) [65]:

$$E(X) = N \times P_T \tag{8}$$

If each SAP has the ability to repair cracks of length equal to the threshold L_{heal}, the expected length of repairing the crack by N number of SAP can be written by $L_{heal} \times E(X)$. The total length of cracks in the material is L_T. If those cracks can be completely healed, the following formulation should be fulfilled:

$$L_{heal} \times E(X) \geq L_T \tag{9}$$

Hence, using Eq. (8) into Eq. (9), healing capacity of SAP intersected the crack lines (L_H) can be given by Lin et al. (2018) [65]:

$$L_H = L_{heal} \times N_A \times A_T \times P_T \tag{10}$$

where N_A is the ratio of N/A_T. Regarding P_T of buffon needle, several studies reported Eq. (11) [64, 66]:

$$P_T = \frac{2l}{\pi B} \tag{11}$$

where B is the distance between cracks and l is the maximum dimension of SAP particles around the rebar. As reported by Mousavi et al. (2020) [47], this length is between 1.88 mm to 2.78 mm for 0.25% and 1.0% SAP respectively. Higher values for higher SAP% can be attributed to the accumulation of SAP which is similar to higher dosages of nanoparticles. Finally, results of the present study can be justified by Eq. (10), as follows:

a. Higher SAP percentage causes a considerable impact on the healing improvement factor. This can be related to the parameter of $N \times P_T$. By increasing the SAP percentage, the Intersection probability of crack-hitting will be increased so that it causes higher healing possibilities at the rebar-concrete interface (Fig. 26(b)).

b. Statistical results indicate that 28-day healing periods are more efficient as compared to the 14-day healing periods. This can be attributed to the L_{heal}. Additionally, as crack width increases, self-healing capacity decreases which similarly can affect the L_{heal}. There is no specific research on studying the expected crack-repairing length by each SAP particle. As shown in Fig. 26, regarding the pre-cracked concrete surrounding the rebar, there are two main potential zones including (1) zone I around the rebar with a distance of $w/2$; and (2) zone II far from the rebar as compared to zone I . Zone I is more dominant for starting the healing process due to the existence of the calcite layer around the rebar, which is essential for $CaCO_3$ precipitation. Many studies reported the enriched quantity of calcium hydroxide at the rebar-concrete interface, as compared to the bulk cement paste [8, 67, 68], observed by the SEM images as well as the EDS analysis [69]. To explain this phenomenon, Moreau (1973) [70] reported that the cement particles inclined to separate from the matrix, generating a slender zone around the rebar with fewer cement particles and thus more water. This provides a layer in which Ca^{2+} ions can diffuse from outside the interface region, resulting in the formation of the considerable content of calcium hydroxide [70]. As shown in Fig. 27, the domain of zone II is determined by αd_b. This distance is a controlled zone in which concrete cover has a considerable impact on bond strength and failure modes. For concrete without stirrups, the limiting value is reached when $c/d_b \geq 3.0$ [71], while for concrete with a $0.4f'_c$ lateral pressure, the normalized ratio $\tau_{max}/\sqrt{f'_c}$ tends to stop increasing after $c/d_b \geq 2.0$ [72]. The present study suggests the simplified following equations for the first potential healing volume around the rebar (Zone I), and the second scenario which is the developed version of the first scenario (zone I and zone II):

$$(V_{healed})_{zone\ I} = 3.93wd_b[2d_b + w] \tag{12}$$

$$(V_{healed})_{zone\ I+zone\ II} = 5wd_b[5.57d_b - 0.21w] \tag{13}$$

$$(V_{healed})_{zone\ I+zone\ II} > (V_{healed})_{zone\ I} \tag{14}$$

$(V_{healed})_{zone\ I}$ corresponds to the concrete mixtures with medium healing improvement factor, while $(V_{healed})_{zone\ I+zone\ II}$ corresponds to a high healing improvement factor. For instance, for the rebar nominal diameter of 10 mm and the crack width of 0.20 mm, values of 158.77 mm^3 and 556.58 mm^3 are obtained for $(V_{healed})_{zone\ I}$ and $(V_{healed})_{zone\ I+zone\ II}$, respectively. As shown in samples after healing periods in Fig. 28, white powders around the rebar and also at rebar rib places are clear and the content is higher than the bulk matrix. This can clearly confirm the hypothesis presented in Fig. 27, where healing probability at Zone I is higher as compared to Zone II.

c. Regarding AE admixture, the statistical results indicated that AE admixture has a positive impact on the healing improvement factor at the rebar-concrete interface. As shown in Fig. 26(b), AE admixture provides a pore network in the matrix, which makes it easy to transfer water between SAP particles. This clearly increases the parameter L_{heal} in the Eq. (10). The distribution of SAP particles along with AE pores is illustrated in Fig. 29.

It is worth mentioning that the present study is only an initial effort to determine the effect of AE admixture on the self-healing method at the rebar-concrete interface. More research is needed to understand the optimum structure of the bubble network (volume and spacing) for different dosages of AE admixture and SAP. Moreover, different types of SAP (varied chemical composition) with different water absorptions are necessary to be tested for obtaining optimum SAP+AE-contained concrete. Furthermore, as mentioned in Eq. (10), results showed that L_{heal} of SAP concrete can be improved by the AE network. However, more studies are needed to quantify this parameter as a function of SAP percentage and AE dosage. Additionally, future works need to extend the research on using the "Buffon needle problem" for optimizing the SAP-AE combination, considering different chemistries.

5 Summary and concluding remarks

This study evaluated the effect of air-entraining admixture on interfacial properties between the steel rebar and un-cracked, pre-cracked, and healed concrete by extensive experimental tests. A comparison study was conducted between AE and non-AE concrete. Two dosages of 0.25% and 1.0% SAP and one dosage of 0.21% AE were considered for the AE-contained mixtures. Results were compared with a recently published paper by authors [47] for non-AE concrete. Additionally, a statistical approach is performed to comprehensively analyse the results. The following critical concluding remarks are drawn from the experimental and statistical results:

- The optimum dosage of 0.25% SAP is obtained for both AE and non-AE mixtures.
- AE admixture is more adaptable with SAP-1 as compared to SAP-2 for uncracked specimens so that AE concrete mixtures containing both 0.25% and 1.0% SAP-1 have similar normalized maximum and residual bond stress, and even higher average bond stress, as compared to the non-AE mixtures.

- Results of uncracked specimens show that SAP type has a significant impact on porosity patterns of AE and non-AE mixtures so that there are some conflicting results between compressive strength results and bond strength results.
- Overall, the results of the pre-cracked specimens show that the pre-cracking phenomenon has higher and more impacts on residual bond stress, as compared to the bond strength.
- AE concrete mixtures are less sensitive to the pre-cracking phenomenon, as compared to the non-AE mixtures.
- Results of the healed specimens show that SAP can improve the self-healing capacity of AE concrete for mitigating damages at the rebar-concrete interface.
- SEM results show that healing products at the external surface of crack have a considerable content of calcium (Ca), while the content is lower than the internal surfaces of cracks.
- It can be deduced from both experimental and statistical results that AE admixture can provide a stabilized bubble network along with SAP locations for improving the self-healing method.

Conflict of interests

The authors declare that there are no competing interests regarding the publication of this paper.

Data Availability Statement

All data, models, and code generated or used during the study appear in the published article.

Acknowledgements

The authors would like to thank ÉTS Montréal technical staff for support in our experiments.

Notation

AE	air-entraining admixture
ANOVA	analysis of variance
B	distance between cracks
d_b	rebar diameter
f'_c	concrete compressive strength
GU	general use cement
H	healing period
IF	improvement factor for self-healing method
IF_{τ_m}	healing improvement factor of average bond stress
IF_{τ_u}	healing improvement factor of bond strength
IF_{τ_r}	healing improvement factor of residual bond stress
IF_{ave}	average healing improvement factor
L_{heal}	threshold length of crack healed by SAP
L_T	total length of cracks in the material
L_H	healing capacity of SAP intersected the crack lines
l	maximum dimension of SAP particles around the rebar
N	number of SAP particles passing cracking path
NC	normal concrete
P_T	crack-hitting probabilities by SAP
RH	relative humidity
SAP	superabsorbent polymer
$SAP\%$	percentage of SAP used by weight of cement
SEM/EDS	scanning electron microscopy/energy dispersive X-ray spectrometry
w	initial crack width
w/d_b	initial crack width-to-rebar diameter ratio
W_T/c	total water-to-cement ratio
X	total number of intersection in the area
τ_m	average bond stress
$\tau_m{}^*$	normalized average bond stress
τ_u	maximum bond stress (or bond strength)
$\tau_u{}^*$	Normalized bond strength
τ_r	residual bond stress
$\tau_r{}^*$	normalized residual bond stress
$(\tau)_c$	bond properties of pre-cracked specimen
$(\tau)_{un}$	bond properties of uncracked specimen
$\tau_{Uncracked}$	bond properties of intact specimens
$\tau_{Precracked}$	bond properties of pre-cracked specimens
τ_{Healed}	bond properties of healed specimens

References

[1] M. Papadrakakis, M. Fragiadakis, N.D. Lagaros, Computational methods in earthquake engineering, Springer2011.

[2] M. Saatcioglu, J.M. Alsiwat, G. Ozcebe, Hysteretic behavior of anchorage slip in R/C members, Journal of Structural Engineering 118(9) (1992) 2439-2458.

[3] M.I. Mousa, Effect of bond loss of tension reinforcement on the flexural behaviour of reinforced concrete beams, HBRC journal 12(3) (2016) 235-241.

[4] P.S. Lobo, J. Almeida, L. Guerreiro, Bond-slip effect in the assessment of RC structures subjected to seismic actions, Procedia Engineering 114 (2015) 792-799.

[5] M.M. Fallah1a, A. Shooshtari1b, H.R. Ronagh, Investigating the effect of bond slip on the seismic response of RC structures, Structural Engineering and Mechanics 46(5) (2013) 695-711.

[6] K. Cashell, A. Elghazouli, B. Izzuddin, Failure assessment of lightly reinforced floor slabs. I: Experimental investigation, Journal of structural engineering 137(9) (2011) 977-988.

[7] S. Mousavi, M. Dehestani, Implementation of bond-slip effects on behaviour of slabs in structures, Computers and Concrete 16(2) (2015) 311-327.

[8] F. Chen, C.Q. Li, H. Baji, B. Ma, Effect of design parameters on microstructure of steel-concrete interface in reinforced concrete, Cement and Concrete Research 119 (2019) 1-10.

[9] I.P. Sfikas, K.G. Trezos, Effect of composition variations on bond properties of self-compacting concrete specimens, Construction and building materials 41 (2013) 252-262.

[10] S.S. Mousavi, S.S. Mousavi Ajarostaghi, C. Bhojaraju, A critical review of the effect of concrete composition on rebar–concrete interface (RCI) bond strength: A case study of nanoparticles, SN Applied Sciences 2(5) (2020) 893.

[11] S.S. Mousavi, L. Guizani, C. Bhojaraju, C. M.Ouellet-Plamondon, Effect of concrete

workability on bond properties of steel rebar in pre-cracked concrete, Proceedings of the Institution of Civil Engineers - Structures and Buildings 0(0) 1-34.

[12] K.H. Mo, U.J. Alengaram, M.Z. Jumaat, Bond properties of lightweight concrete–a review, Construction and Building Materials 112 (2016) 478-496.

[13] S.-W. Kim, H.-D. Yun, Influence of recycled coarse aggregates on the bond behavior of deformed bars in concrete, Engineering Structures 48 (2013) 133-143.

[14] K.M.A. Hossain, M. Lachemi, Bond behavior of self-consolidating concrete with mineral and chemical admixtures, Journal of Materials in Civil Engineering 20(9) (2008) 608-616.

[15] V.S. Ramachandran, Concrete admixtures handbook: properties, science and technology, William Andrew, Park Ridge, New Jersey, 1996.

[16] P. Usher, J. Angles, R. Rixom, R. Ryle, Guide to Chemical Admixtures for Concrete (Technical Report No. 18), London, 1980, pp. The Cement Admixtures Association, Concrete Society.

[17] Y. Şahin, Y. Akkaya, F. Boylu, M. Taşdemir, Characterization of air entraining admixtures in concrete using surface tension measurements, Cement and Concrete Composites 82 (2017) 95-104.

[18] X. Ouyang, Y. Guo, X. Qiu, The feasibility of synthetic surfactant as an air entraining agent for the cement matrix, Construction and Building Materials 22(8) (2008) 1774-1779.

[19] C. Chantrelle, S.S. Mousavi, C.M. Ouellet-Plamondon, Effect of chemical admixtures on rheology, hydration and strength, 10th ACI/Rilem conference on cementitious materials and alternative binders for sustainable, Montréal, QC, Canada, 2017.

[20] B. Łaźniewska-Piekarczyk, The type of air-entraining and viscosity modifying admixtures and porosity and frost durability of high performance self-compacting concrete, Construction and

Building Materials 40 (2013) 659-671.

[21] D. St John, A. Poole, I. Sims, Concrete petrography: a handbook of investigative techniques (2nd ed.), CRC Press, London, 1998.

[22] W.L. Dolch, Air-entraining admixtures, in: V.S.R. (Ed.) (Ed.), Concrete Admixtures Handbook: Properties, Science, and Technology (2nd Edition), Elsevier1996, pp. 518-557.

[23] G. Bruere, Fundamental actions of air-entraining agents, International Symposium on Admixture for Mortar and Concrete, RILEM Publications, Brussels, Belgium, 1967, pp. 7-23.

[24] R.C. Mielenz, Use of surface-active agents in concrete, Fifth International Symposium on Chemistry of Cement, Tokyo, 1968, pp. 22-24.

[25] R. Dhir, M. McCarthy, M. Limbachiya, I. El Sayad, D. Zhang, Pulverized fuel ash concrete: air entrainment and freeze/thaw durability, Magazine of Concrete Research 51(1) (1999) 53-64.

[26] H. Shang, Y. Song, J. Ou, Behavior of air-entrained concrete after freeze-thaw cycles, Acta Mechanica Solida Sinica 22(3) (2009) 261-266.

[27] W. Perenchio, V. Kress, D. Breitfeller, Frost Lenses? Sure, but in Concrete?, Concrete International 12(4) (1990) 51-53.

[28] H. Ma, H. Yu, C. Li, Y. Tan, W. Cao, B. Da, Freeze–thaw damage to high-performance concrete with synthetic fibre and fly ash due to ethylene glycol deicer, Construction and Building Materials 187 (2018) 197-204.

[29] M.Y. Hang, W. Zhang, Efficiency air-entraining water-reducing agent in concrete study on the freeze-thaw resistance, Applied Mechanics and Materials, Trans Tech Publ, 2011, pp. 3566-3571.

[30] G.-F. Peng, Q. Ma, H.-M. Hu, R. Gao, Q.-F. Yao, Y.-F. Liu, The effects of air entrainment and pozzolans on frost resistance of 50–60 MPa grade concrete, Construction and Building

Materials 21(5) (2007) 1034-1039.

[31] H. Ziari, P. Hayati, J. Sobhani, Air-entrained air field self-consolidating concrete pavements: strength and durability, International Journal of Civil Engineering 15(1) (2017) 21-33.

[32] X.H. Zheng, Y. Ge, J. Yuan, Influence of air content and vibration time on frost resistance of air entrained concrete, Advanced Materials Research, Trans Tech Publ, 2014, pp. 110-115.

[33] X.L. Yuan, B.X. Li, S.H. Zhou, Freeze-thaw and de-icing salt resistance of concrete containing mineral admixtures and air-entraining agent, Advanced Materials Research, Trans Tech Publ, 2011, pp. 3122-3127.

[34] R. Dhir, M. Jones, H. Ahmed, A. Seneviratne, Rapid estimation of chloride diffusion coefficient in concrete, Magazine of Concrete Research 42(152) (1990) 177-185.

[35] R. Dhir, M. Jones, A. Senerirathe, Diffusion of chlorides into concrete influence of PFA quality, Cement and concrete research 21(6) (1991) 1092-1102.

[36] P.-C. Aïtcin, Entrained air in concrete: Rheology and freezing resistance, Woodhead Publishing2016.

[37] R. Gagné, Air entraining agents, Science and Technology of Concrete Admixtures, Elsevier2016, pp. 379-391.

[38] J. Han, H. Fang, K. Wang, Design and control shrinkage behavior of high-strength self-consolidating concrete using shrinkage-reducing admixture and super-absorbent polymer, Journal of sustainable cement-based materials 3(3-4) (2014) 182-190.

[39] C. Shi, J. Liu, K. Lv, X. Ma, J. Zhang, Z. Wu, Effect of Super-Absorbent Polymer on Shrinkage and Permeability of Self-Compacting Concrete (SCC), 8th International RILEM Symposium on Self-Compacting Concrete, Washington, D.C., 2016, pp. 73-88.

[40] H. AzariJafari, A. Kazemian, M. Rahimi, A. Yahia, Effects of pre-soaked super absorbent

polymers on fresh and hardened properties of self-consolidating lightweight concrete, Construction and Building Materials 113 (2016) 215-220.

[41] S. Al-Hubboubi, T. al-Attar, H. Al-Badry, S. Abood, R. Mohammed, B. Haddhood, Performance of super-absorbent polymer as an internal curing agent for self-compacting concrete, MATEC Web of Conferences, EDP Sciences, 2018, p. 02023.

[42] P. Lura, F. Durand, A. Loukili, K. Kovler, O.M. Jensen, Compressive strength of cement pastes and mortars with superabsorbent polymers, Proceedings of the International RILEM Conference on Volume Changes of Hardening Concrete: Testing and Mitigation, Rilem Publications SARL Lyngby, 2006, pp. 117-125.

[43] K. Farzanian, K.P. Teixeira, I.P. Rocha, L.D.S. Carneiro, A. Ghahremaninezhad, The mechanical strength, degree of hydration, and electrical resistivity of cement pastes modified with superabsorbent polymers, Construction and Building Materials 109 (2016) 156-165.

[44] K. Van Tittelboom, J. Wang, M. Araújo, D. Snoeck, E. Gruyaert, B. Debbaut, H. Derluyn, V. Cnudde, E. Tsangouri, D. Van Hemelrijck, Comparison of different approaches for self-healing concrete in a large-scale lab test, Construction and Building Materials 107 (2016) 125-137.

[45] D. Snoeck, K. Van Tittelboom, N. De Belie, S. Steuperaert, P. Dubruel, The use of superabsorbent polymers as a crack sealing and crack healing mechanism in cementitious materials, Concrete Repair, Rehabilitation and Retrofitting III: 3rd International Conference on Concrete Repair, Rehabilitation and Retrofitting, ICCRRR-3, 3–5 September 2012, CRC Press Cape Town, South Africa, 2012, p. 58.

[46] D. Snoeck, K. Van Tittelboom, S. Steuperaert, P. Dubruel, N. De Belie, Self-healing cementitious materials by the combination of microfibres and superabsorbent polymers, Journal of Intelligent Material Systems and Structures 25(1) (2014) 13-24.

[47] S.S. Mousavi, C.M. Ouellet-Plamondon, L. Guizani, C. Bhojaraju, V. Brial, On mitigating rebar–concrete interface damages due to the pre-cracking phenomena using superabsorbent polymers, Construction and Building Materials 253 (2020) 119181.

[48] S. Mousavi, C. Ouellet-Plamondon, L. Guizani, Effect of superabsorbent polymer on mitigating damages at steel bar-concrete interface, CSCE Annual Conference, Laval (Greater Montreal), 2019.

[49] S.S. Mousavi, L. Guizani, C.M. Ouellet-Plamondon, On bond-slip response and development length of steel bars in pre-cracked concrete, Construction and Building Materials 199 (2019) 560-573.

[50] S.S. Mousavi, L. Guizani, C.M. Ouellet-Plamondon, Simplified Analytical Model for Interfacial Bond Strength of Deformed Steel Rebars Embedded in Pre-cracked Concrete, Journal of Structural Engineering 146(8) (2020) 04020142.

[51] F. Brantschen, D. Faria, M. Fernández Ruiz, A. Muttoni, Bond behaviour of straight, hooked, U-shaped and headed bars in cracked concrete, Structural Concrete 17(5) (2016) 799-810.

[52] P. Desnerck, J.M. Lees, C.T. Morley, Bond behaviour of reinforcing bars in cracked concrete, Construction and Building Materials 94 (2015) 126-136.

[53] T. Rilem, RILEM recommendations for the testing and use of constructions materials, RC 6 (1994) 218-220.

[54] S.S. Mousavi, L. Guizani, C. Bhojaraju, C.M. Ouellet-Plamondon, Effect of concrete workability on bond properties of steel rebar in pre-cracked concrete, Proceedings of the Institution of Civil Engineers-Structures and Buildings (2020) 1-34.

[55] S. Mousavi, M. Dehestani, K. Mousavi, Bond strength and development length of steel bar in unconfined self-consolidating concrete, Engineering Structures 131 (2017) 587-598.

[56] S. Mousavi, M. Dehestani, S. Mousavi, Bond strength and development length of glass fiber-reinforced polymer bar in unconfined self-consolidating concrete, Journal of Reinforced Plastics and Composites 35(11) (2016) 924-941.

[57] S. Gupta, H.W. Kua, S.D. Pang, Combination of polypropylene fibre and superabsorbent polymer to improve physical properties of cement mortar, Magazine of Concrete Research 70(7) (2018) 350-364.

[58] H.W. Kua, S. Gupta, A.N. Aday, W.V. Srubar III, Biochar-immobilized bacteria and superabsorbent polymers enable self-healing of fiber-reinforced concrete after multiple damage cycles, Cement and Concrete Composites 100 (2019) 35-52.

[59] S. Ahmad, K. Pilakoutas, M.M. Rafi, Q.U.Z. Khan, K. Neocleous, Experimental investigation of bond characteristics of deformed and plain bars in low strength concrete, Scientia Iranica 25(6) (2018) 2954-2966.

[60] I. Minitab, Minitab (Version release 17) [Statistical Computer Software], Minitab, Inc. , State College, PA, 2014.

[61] I.N.C. StatSoft, STATISTICA, data analysis software system (Version 10) [Computer software], StatSoft Inc., Tulsa, Oklahoma.

[62] D. Snoeck, N. De Belie, Autogenous healing in strain-hardening cementitious materials with and without superabsorbent polymers: an 8-year study, Frontiers in Materials 6 (2019).

[63] D. Snoeck, T. De Schryver, N. De Belie, Enhanced impact energy absorption in self-healing strain-hardening cementitious materials with superabsorbent polymers, Construction and Building Materials 191 (2018) 13-22.

[64] C. Chung, Application of the Buffon needle problem and its extensions to parallel-line search sampling scheme, Journal of the International Association for Mathematical Geology 13(5) (1981)

371-390.

[65] J. Lin, H. Chen, Z. Lv, Y. Wang, Analytical solution on dosage of self-healing capsules in materials with two-dimensional multi-shaped crack patterns, Science and Engineering of Composite Materials 25(6) (2018) 1229-1239.

[66] I.G. Johannesen, The Buffon needle problem revisited in a pedagogical perspective, Mathematica Journal 11(2) (2008) 284.

[67] A. Horne, I. Richardson, R. Brydson, Quantitative analysis of the microstructure of interfaces in steel reinforced concrete, Cement and Concrete Research 37(12) (2007) 1613-1623.

[68] L. Yue, H. Shuguang, The microstructure of the interfacial transition zone between steel and cement paste, Cement and Concrete Research 31(3) (2001) 385-388.

[69] S. Arya, B. Das, S.K. Goudar, Microstructural Study of Steel-Concrete Interface and Its Influence on Bond Strength of Reinforced Concrete, Advances in Civil Engineering Materials 8(1) (2019) 171-189.

[70] M. Moreau, Contribution to the study of adhesion between the hydrated constituents of artificial Portland cement and embedded steel, Revenue mater 674 (1973) 4-17.

[71] Y.-F. Wu, X.-M. Zhao, Unified bond stress–slip model for reinforced concrete, Journal of Structural Engineering 139(11) (2012) 1951-1962.

[72] P. Walker, M. Batayneh, P. Regan, Bond strength tests on deformed reinforcement in normal weight concrete, Materials and Structures 30(7) (1997) 424.

List of Tables:

Table 1 Concrete composition of AE concrete mixtures

Mix	Cement	Sand	Gravel 5/10	Gravel 10/14	Water	Add. water	SP	AE	SAP
	(kg/m^3)								%
RA-1	395	788	822	258	165	0	3.98	0.83	0
RA-2	395	788	822	258	165	0	5.23	0.83	0
25S1A	395	788	822	258	165	24.7	3.27	0.83	0.25
25S2A	395	788	822	258	165	24.7	2.23	0.83	0.25
100S1A	395	788	822	258	165	98.8	4.15	0.83	1.0

* Note: Add=additional water, SP=superplasticizer by MasterGlenium 1466 for all mixture except mixes RA-1 and 100S1A which used EUCON PLASTOL 341, SAP= % wt. of cement, AE=air entraining by Eucon air mac 6 (0.21% wt. of cement).

Table 2 Configurations of mixtures

Mixture	AE		Polymer		SAP percentage (%)				W_T/c	Slump (mm)	Density[1] (kg/m^3)
	With	Without	SAP-1	SAP-2	0	0.25	0.50	1.00			
R		×			×				0.41	97	2453.80
RA-1	×				×				0.41	110	-
RA-2	×				×				0.43	200	2390.08
25S1		×	×			×			0.48	104	2416.79
25S1A	×		×			×			0.48	170	2368.02
25S2		×		×		×			0.48	109	2419.22
25S2A	×			×		×			0.48	191	2283.30
50S1		×	×				×		0.54	95	2335.76
100S1		×	×					×	0.66	91	2256.72
100S1A	×		×					×	0.66	100	2219.85

* Note: W_T/c= total water-to-cement ratio.[1] average hardened density of mixtures after 28 days curing.

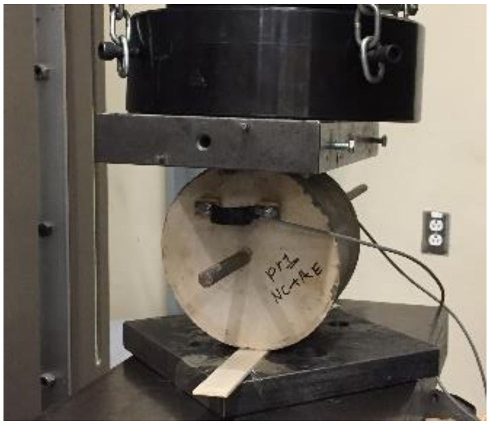

(a)

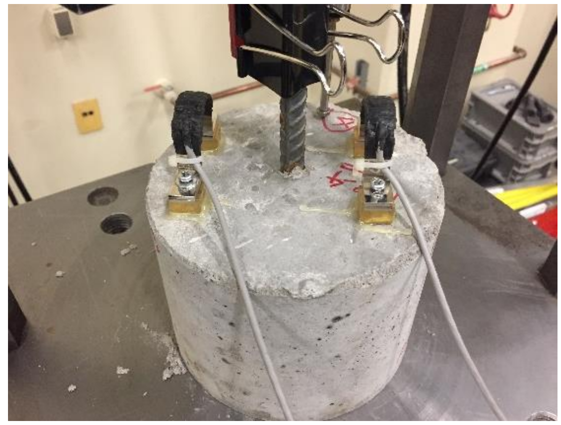

(b)

(c)

Fig. 1 Experimental procedure:
(a) pre-cracking test; (b) pull-out test; (c) heat-shrinkable tube

(a) (b)

Fig. 2 Failure modes for pull-out test specimens: (a) pull-out failure; (b) splitting failure

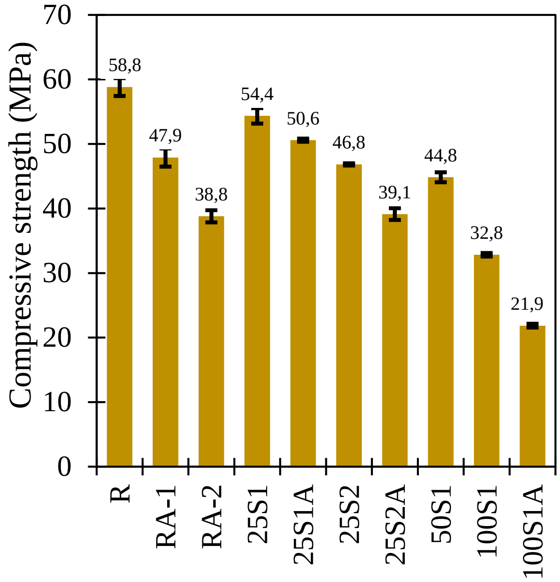

(a)

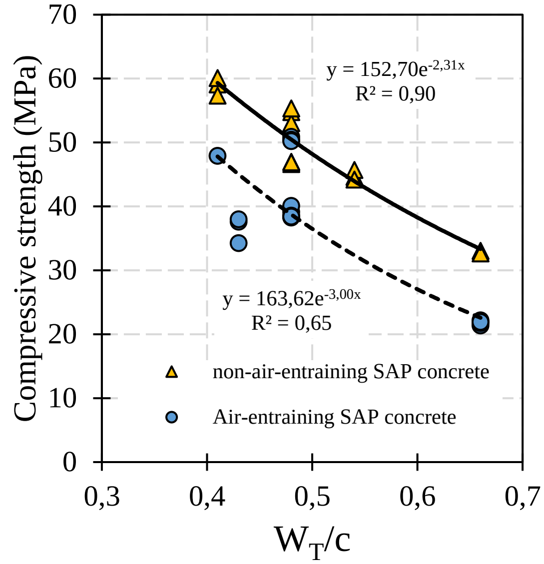

(b)

Fig. 3 Compressive strength of concrete mixtures containing SAP and AE

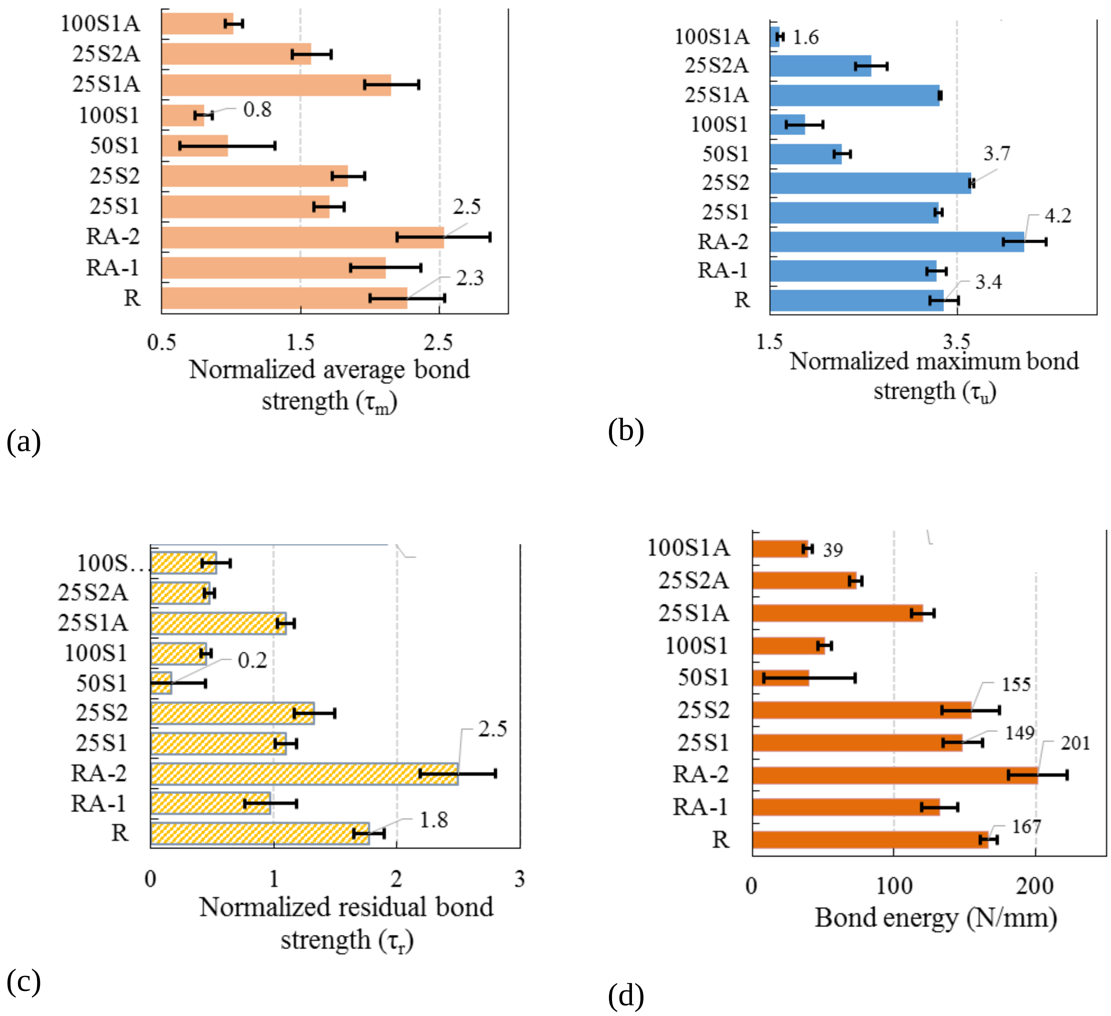

Fig. 4 Normalized bond properties of mixtures: (a) average bond stress; (b) bond strength; (c) residual bond stress; (d) bond energy

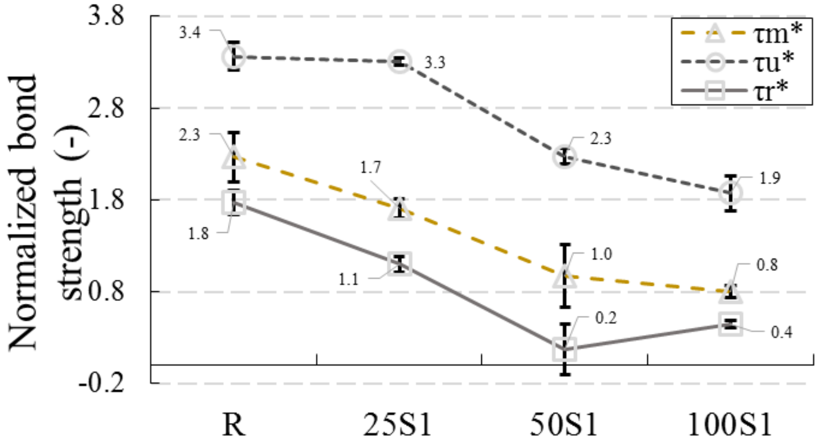

(a)

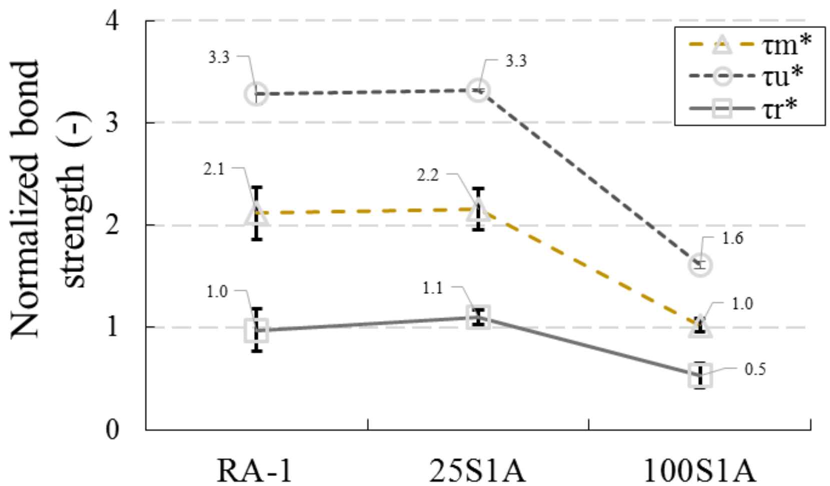

(b)

Fig. 5 Effect of SAP percentage on normalized bond properties of uncracked concrete: (a) non-AE concrete; (b) AE concrete

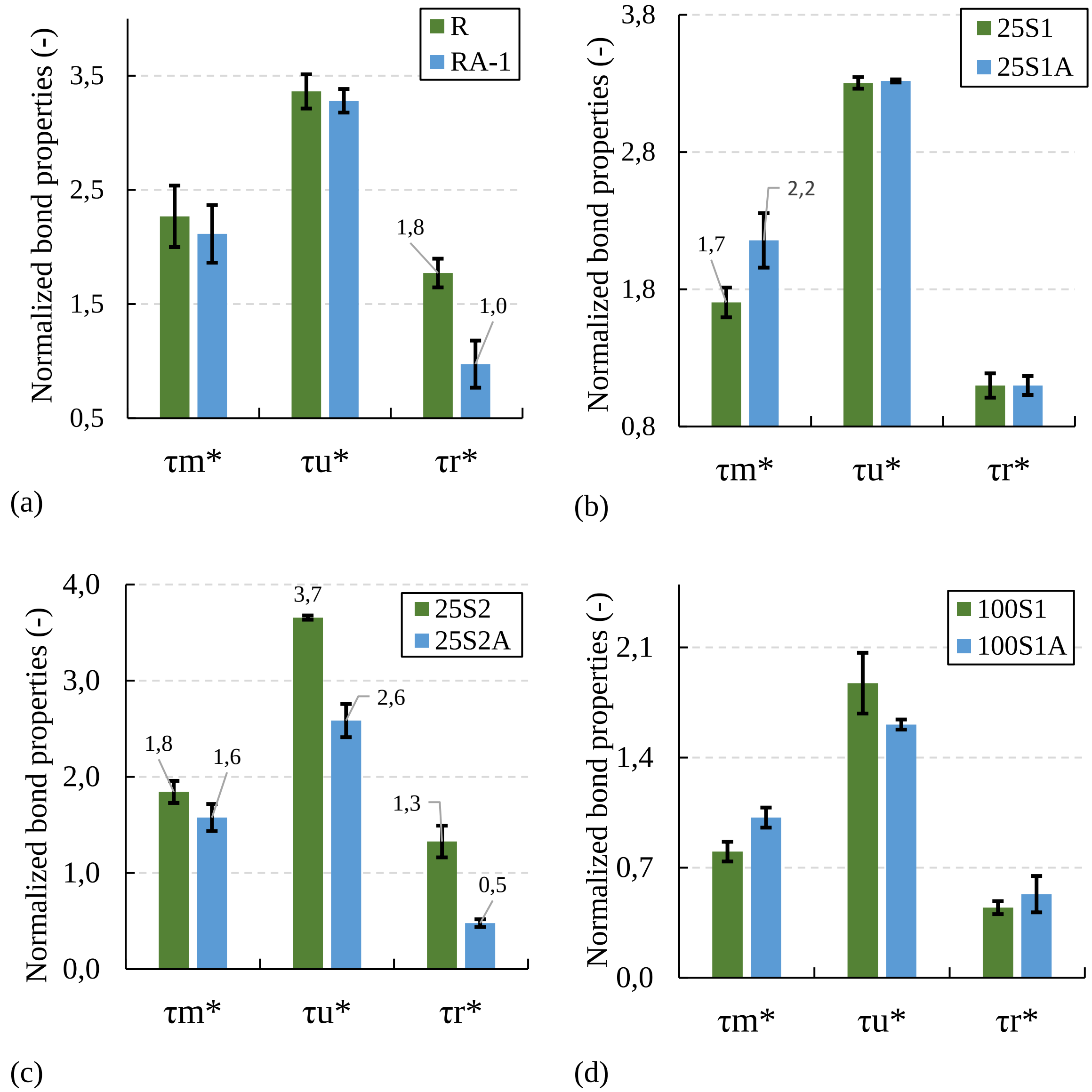

Fig. 6 Effect of AE admixture on normalized bond properties of uncracked concrete: (a) reference mixtures (0% SAP); (b) 0.25% SAP-1; (c) 0.25% SAP-2; (d) 1.0% SAP-1

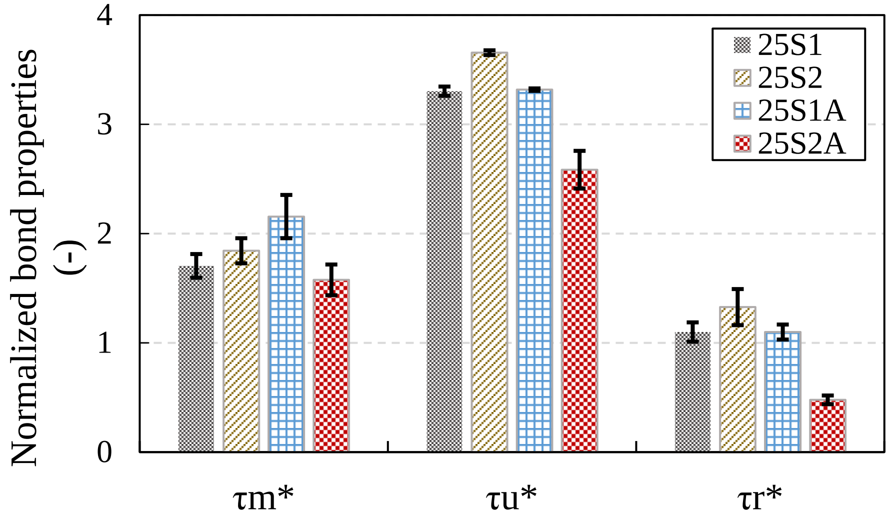

Fig. 7 Effect of SAP type and particle size on normalized bond properties of AE and non-AE uncracked concrete

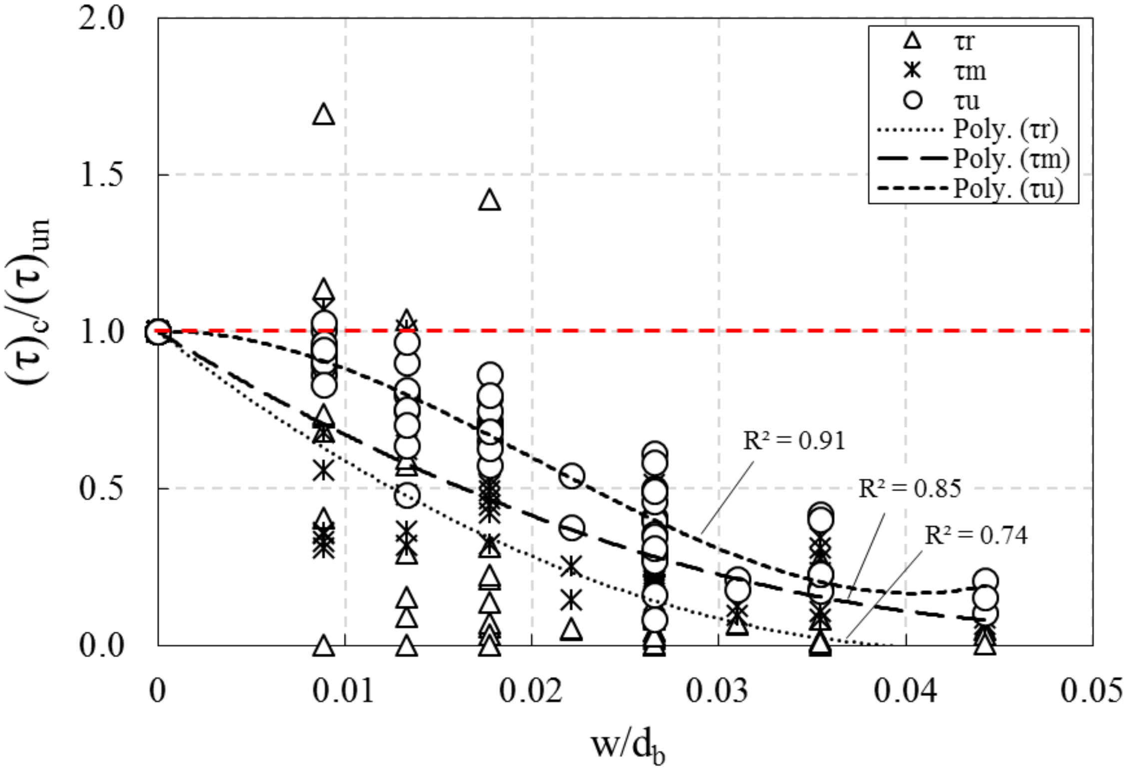

Fig. 8 Effect of the pre-cracking phenomenon on bond properties for all mixtures

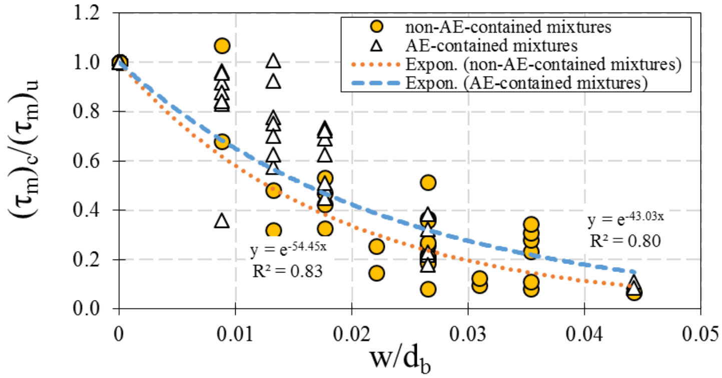

(a)

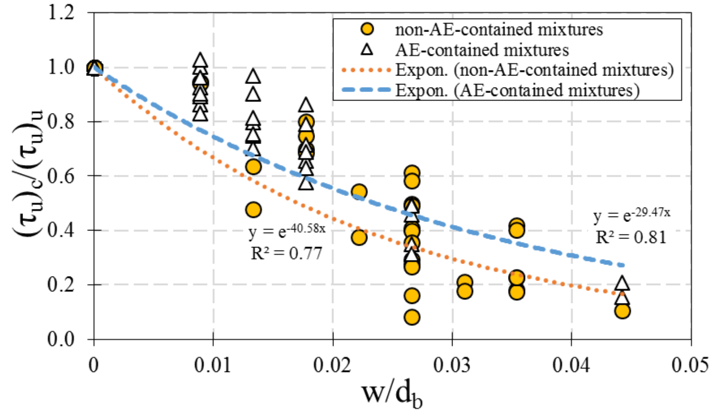

(b)

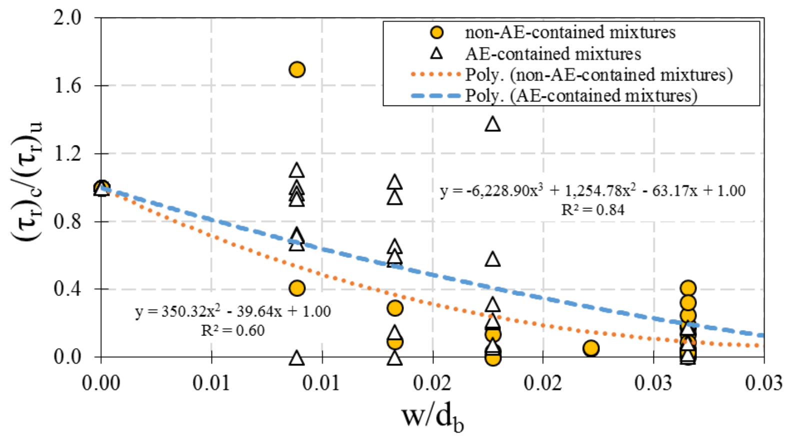

(c)

Fig. 9 Effect of the pre-cracking phenomenon on bond properties with respect to AE admixture: (a) average bond stress; (b) bond strength; (c) residual bond stress

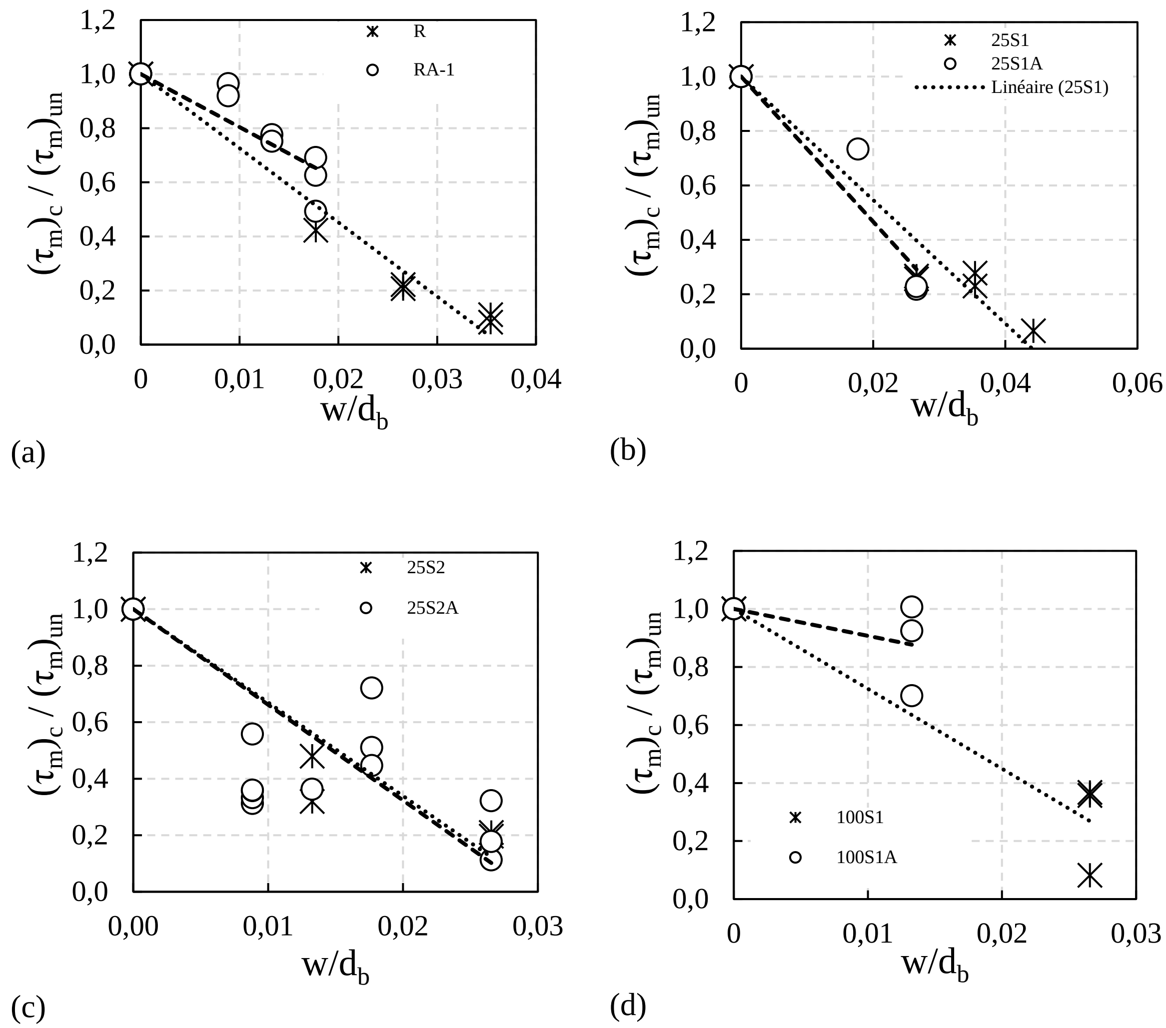

Fig. 10 Effect of AE admixture on the average bond stress of pre-cracked concrete with respect to different SAP percentages: (a) 0% SAP; (b) 0.25% SAP-1; (c) 0.25% SAP-2; (d) 1.0% SAP-1

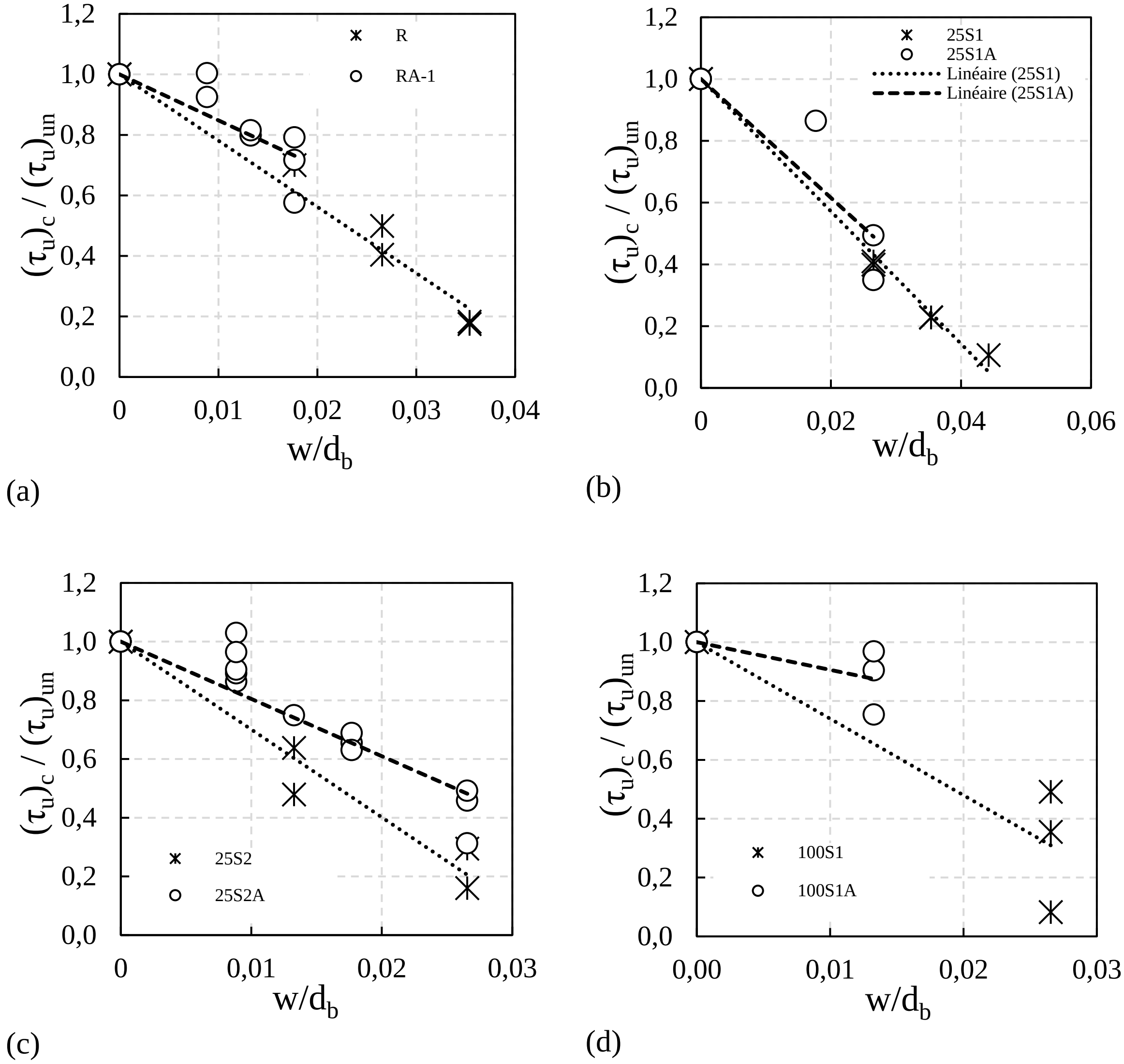

Fig. 10 Effect of AE admixture on the bond strength of pre-cracked concrete with respect to different SAP percentages: (a) 0% SAP; (b) 0.25% SAP-1; (c) 0.25% SAP-2; (d) 1.0% SAP-1

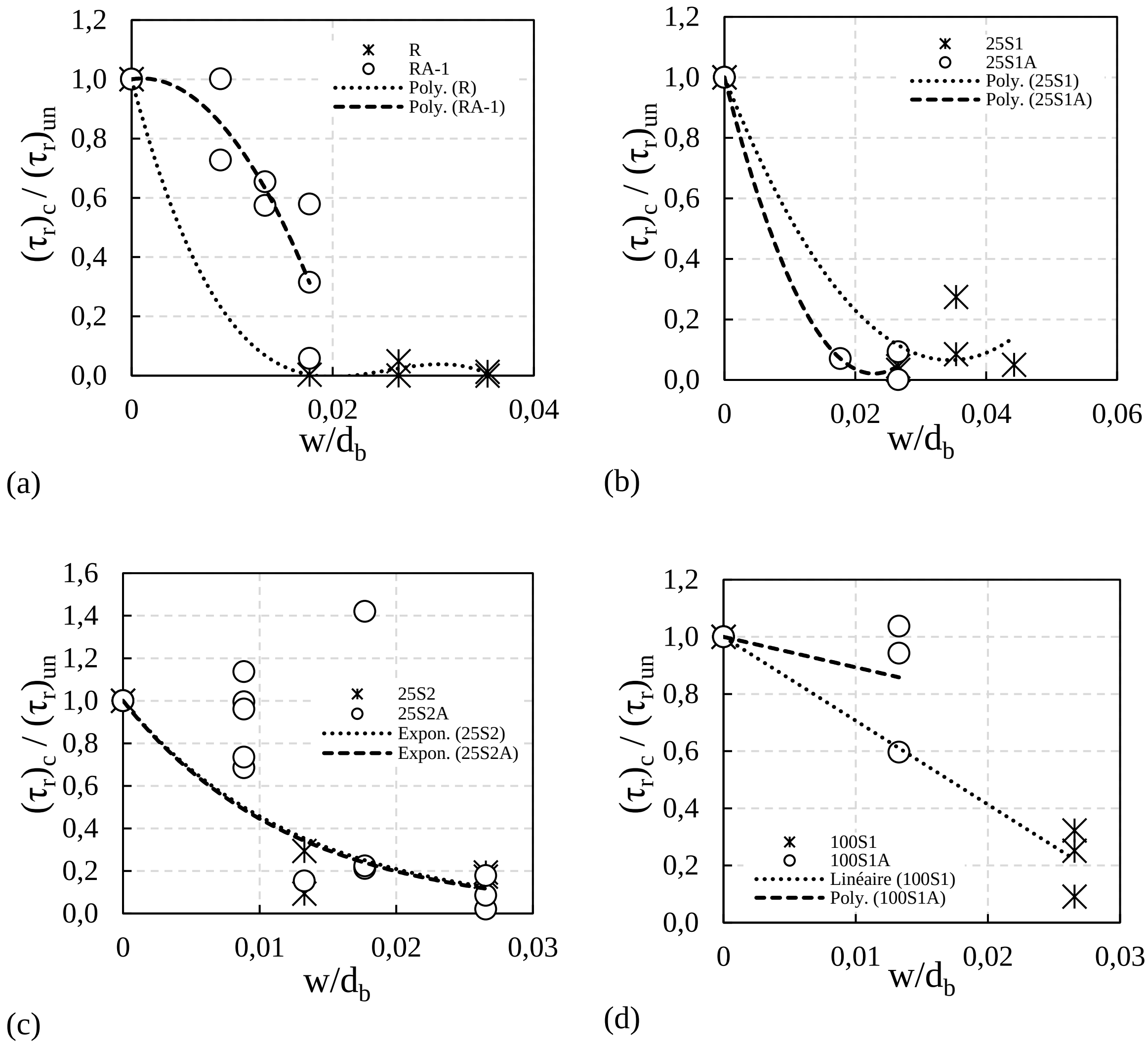

Fig. 11 Effect of AE admixture on the residual bond stress of pre-cracked concrete with respect to different SAP percentages: (a) 0% SAP; (b) 0.25% SAP-1; (c) 0.25% SAP-2; (d) 1.0% SAP-1

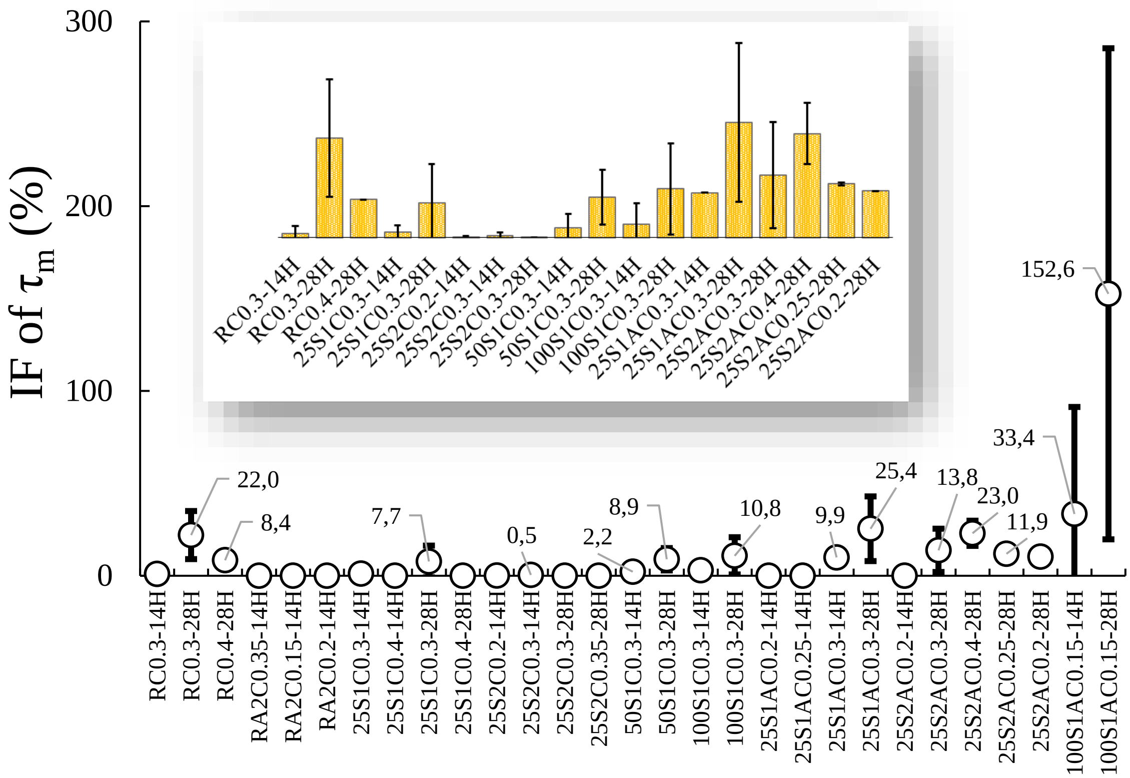

Fig. 12 Determination of IF for average bond stress

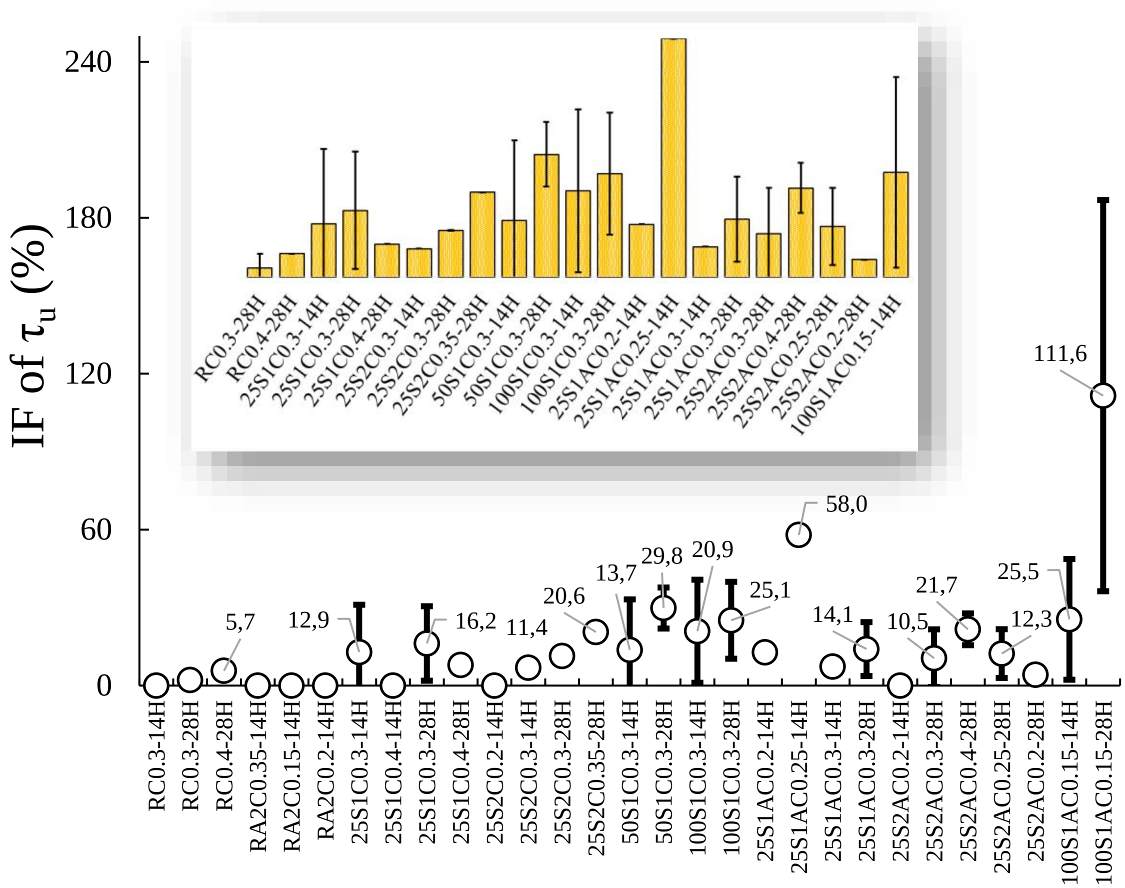

Fig. 13 Determination of IF for bond strength

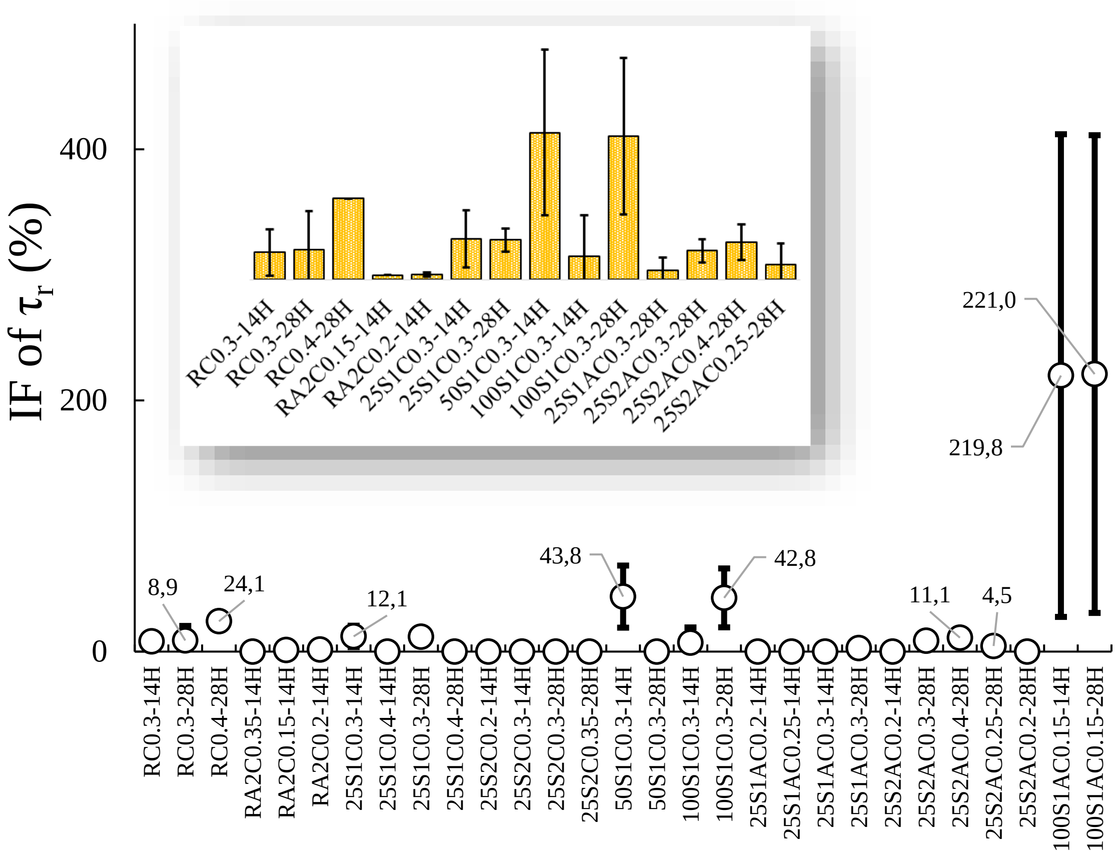

Fig. 14 Determination of IF for residual bond stress

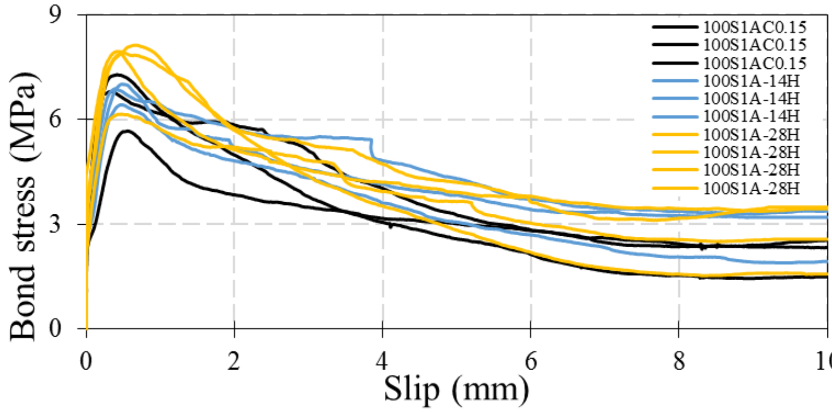

(a) $w = 0.15\ mm$

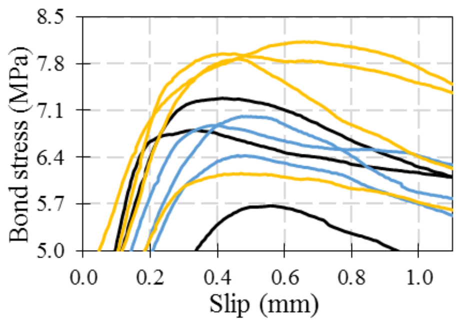

(b)

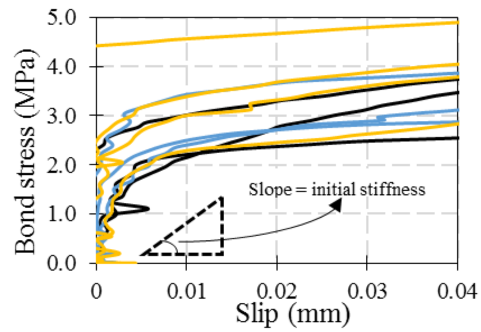

(c)

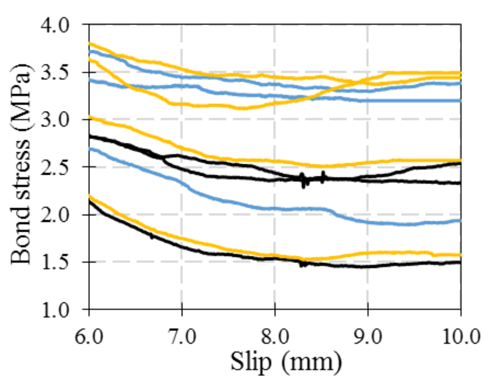

(d)

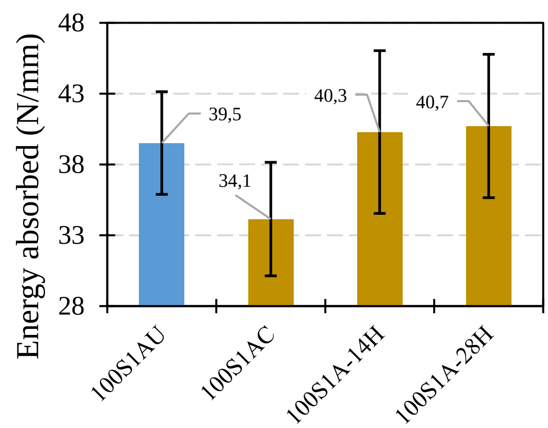

(e)

Fig. 15 Results of 100S1A mixtures: (a) bond-slip curves; (b) bond strength; (c) initial bond stiffness; (d) residual bond stress; (e) energy absorbed

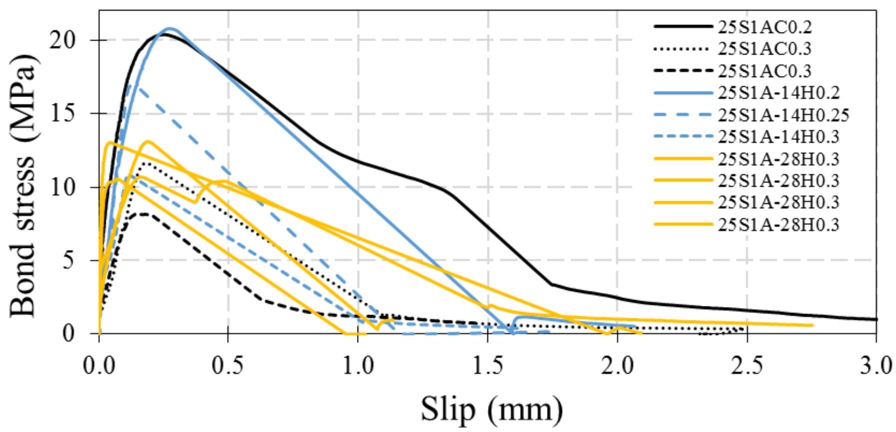

(a) $w = 0.20\ mm, 0.25\ mm, 0.30\ mm$

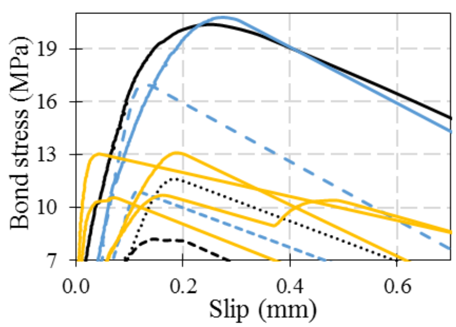

(b)

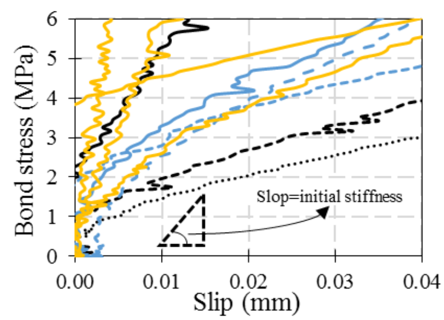

(c)

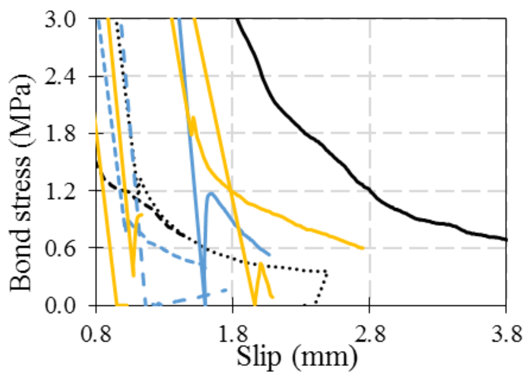

(d)

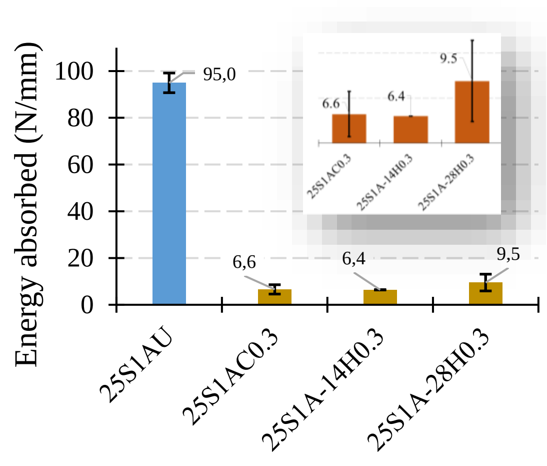

(e)

Fig. 16 Results of 25S1A mixtures: (a) bond-slip curves; (b) bond strength; (c) initial bond stiffness; (d) residual bond stress; (e) energy absorbed

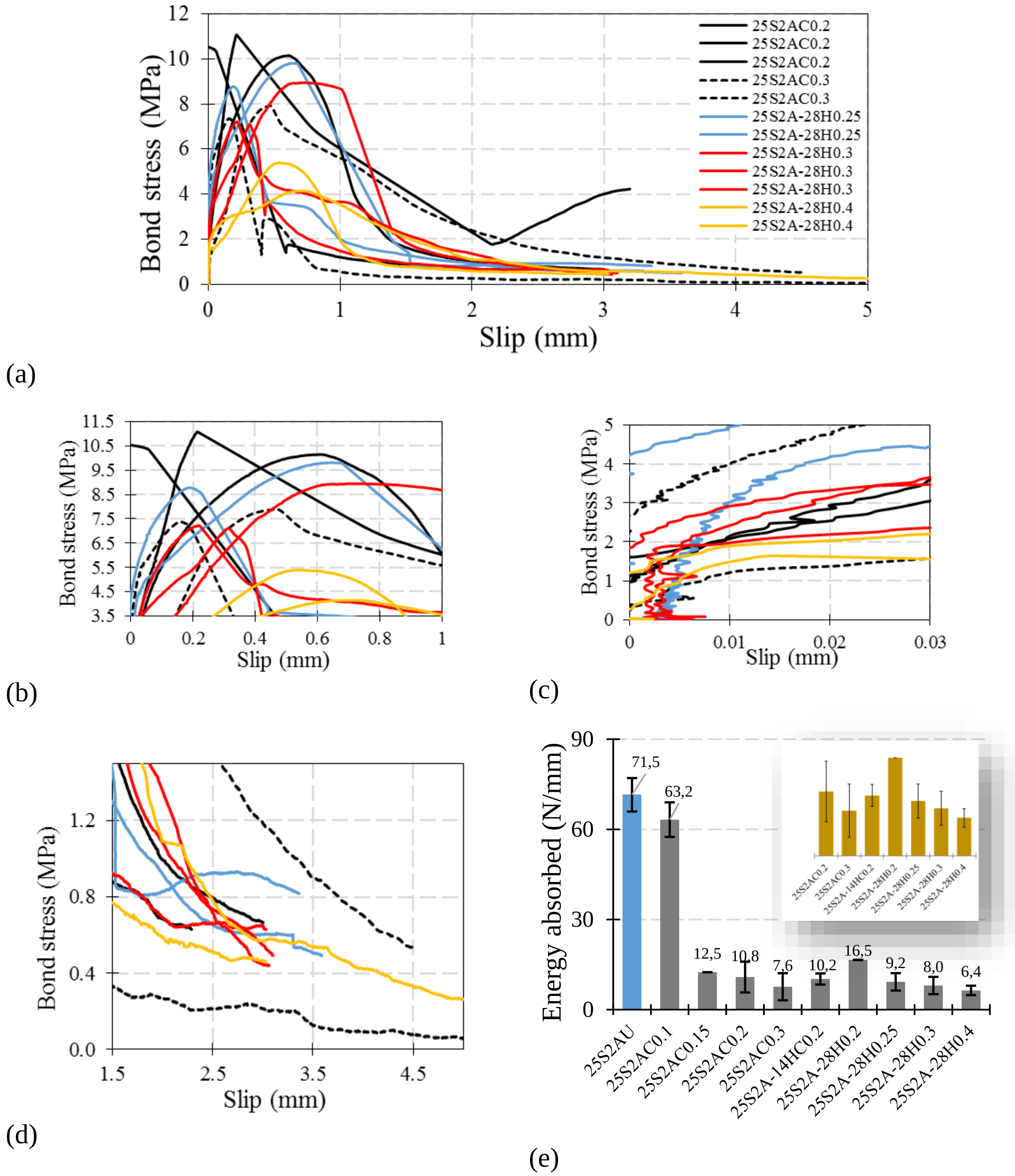

Fig. 17 Results of 25S2A mixtures: (a) bond-slip curves; (b) bond strength; (c) initial bond stiffness; (d) residual bond stress; (e) energy absorbed

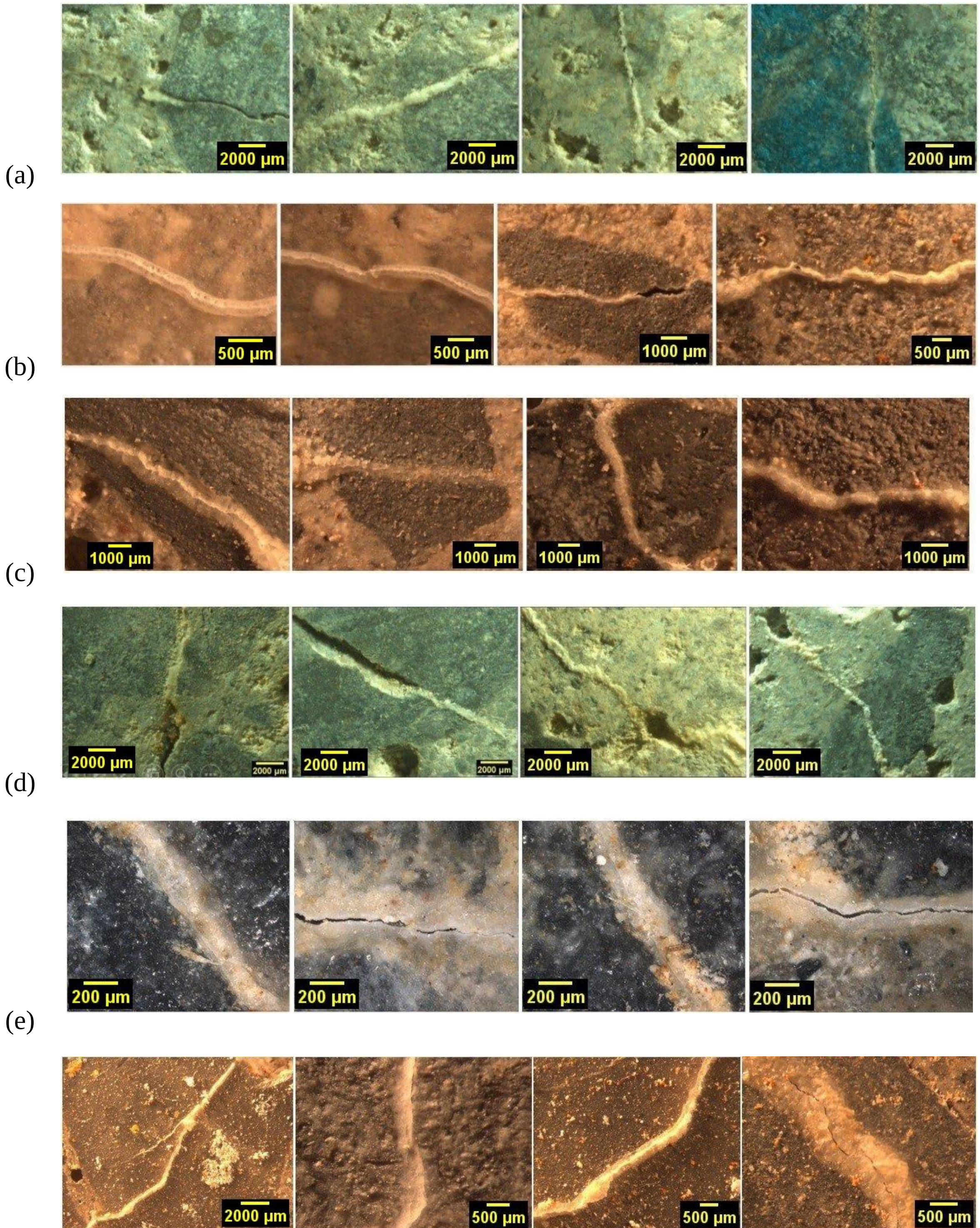

Fig. 18 Self-healing (and/or sealing) products on crack surface after wet-dry cycles: (a) 25S1; (b) 25S2; (c) 25S2A; (d) 50S1; (e) 100S1; (f) 100S1A

Fig. 19 Healing products at the external crack surface of pull-out specimens of SAP-based NC mixtures with and without AE

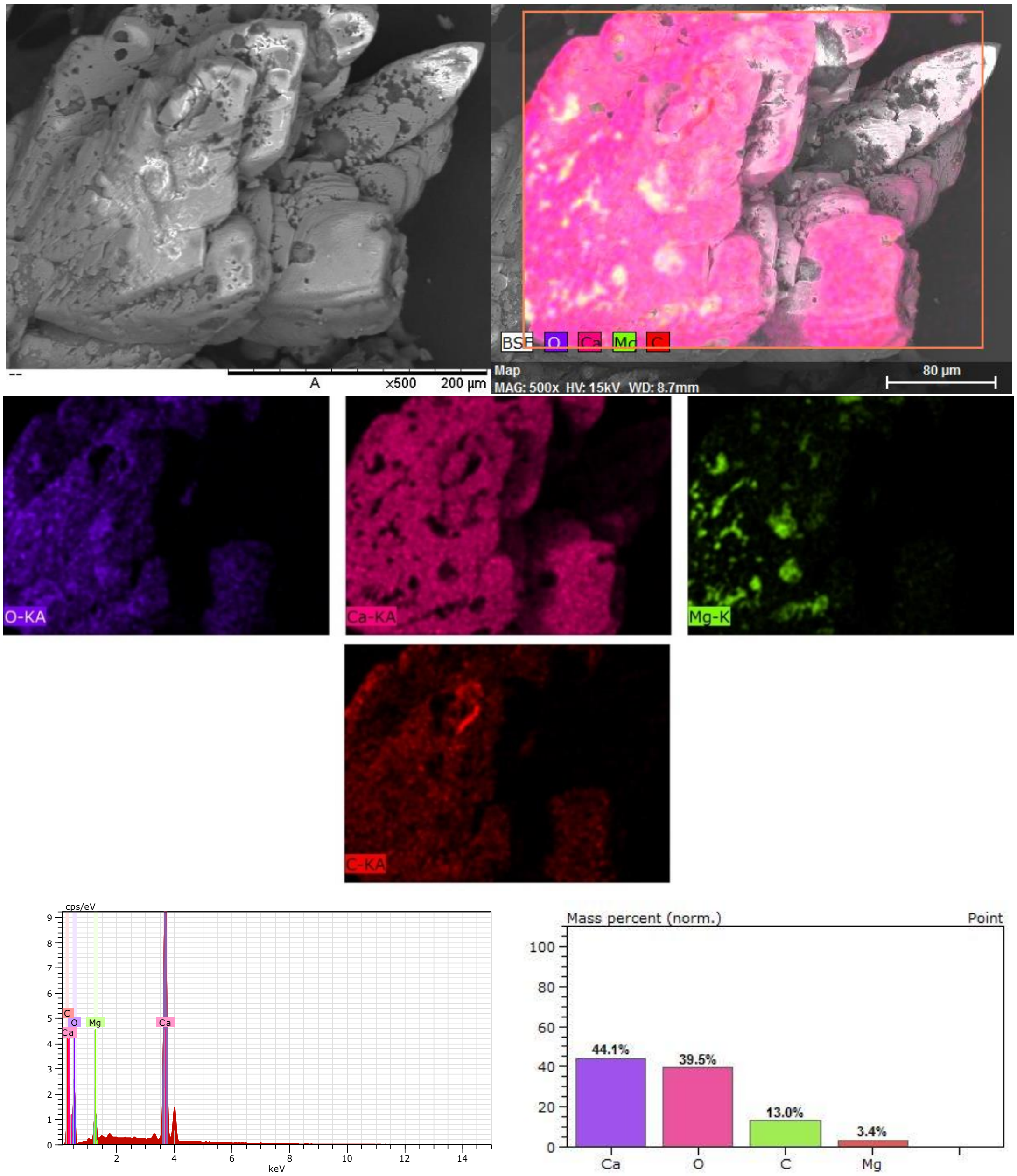

Fig. 20 SEM image analysis of healed products at the external lip of cracks

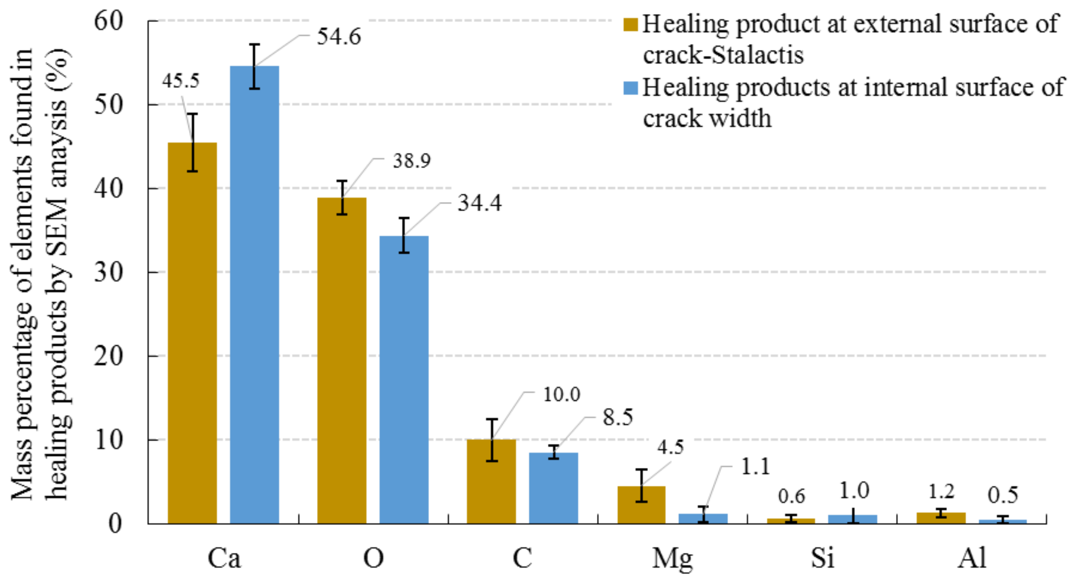

Fig. 21 Comparison of mass percentage of elements found in the healing products at the internal and external surfaces of cracks

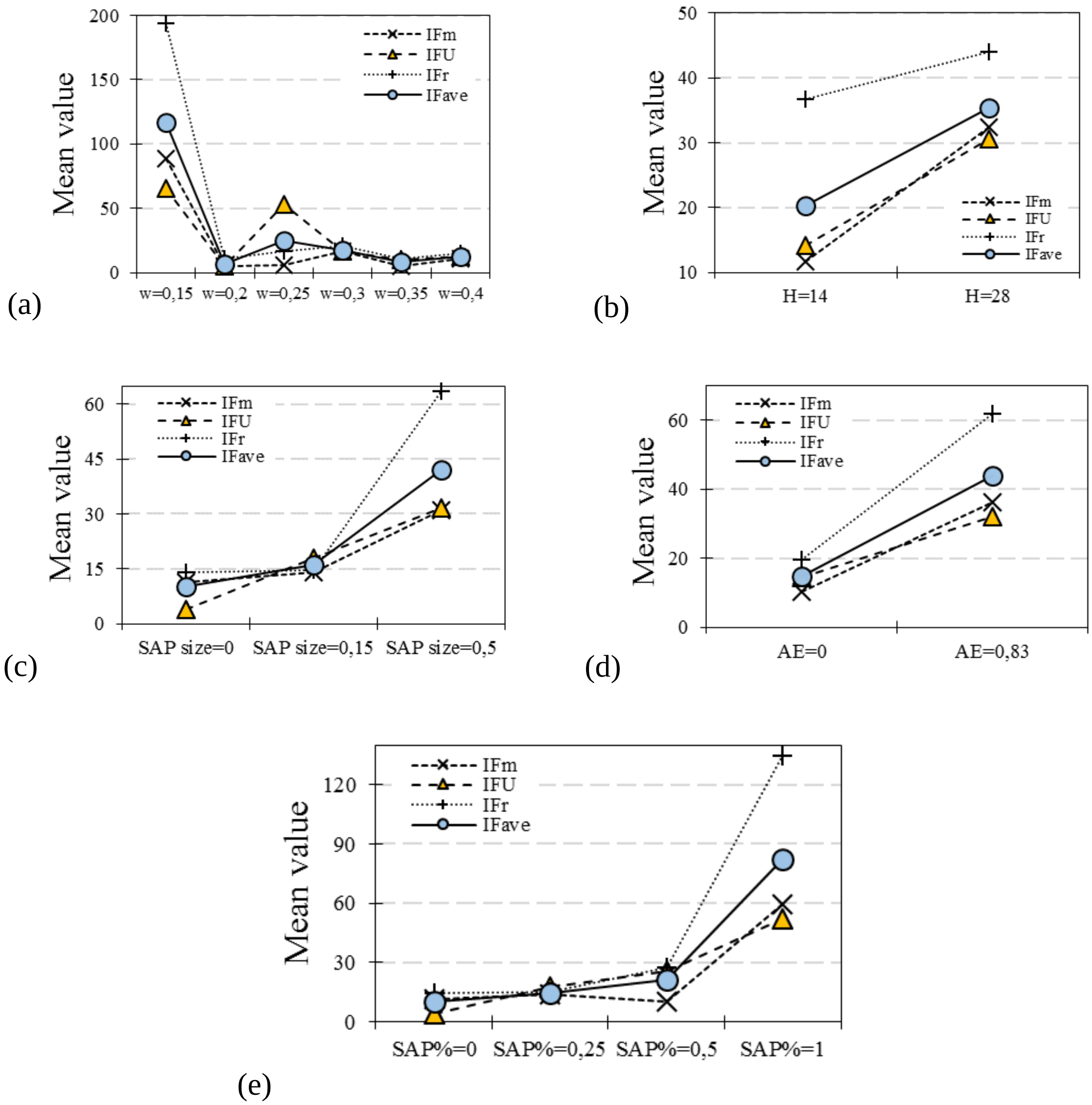

Fig. 22 Main effects plot obtained by ANOVA with respect to: (a) crack width; (b) healing period; (c) SAP size; (d) AE dosage; (e) SAP percentage

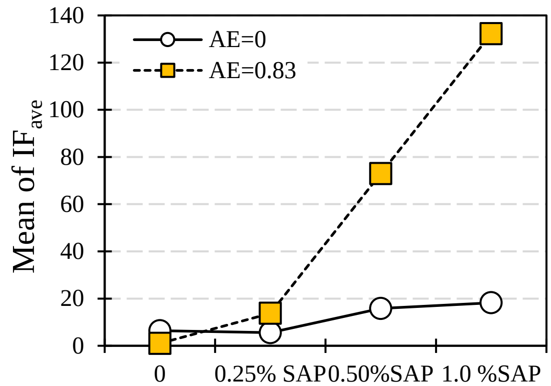

(a)

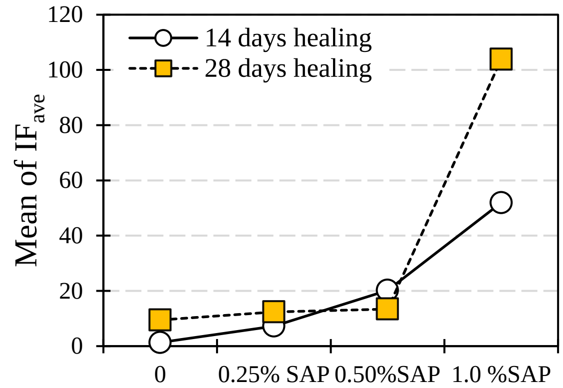

(b)

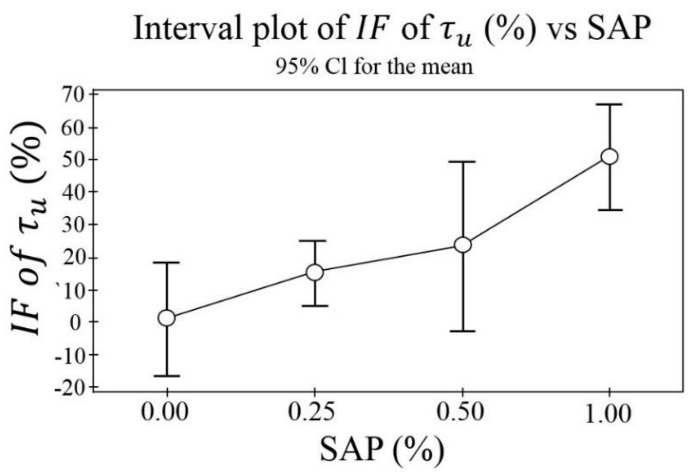

(c)

Fig. Erreur ! Il n'y a pas de texte répondant à ce style dans ce document.**23** Influence of SAP percentage based on ANOVA analysis:
(a) interaction plot with respect to AE; (b) interaction plot with respect to healing period; (c) interval plot of IF_u

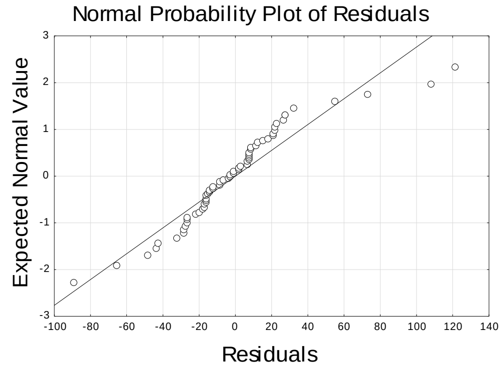

(a)

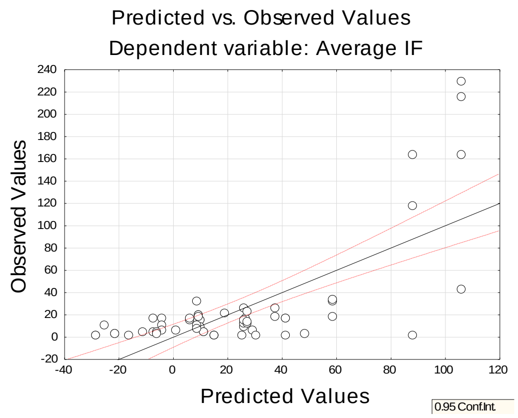

(b)

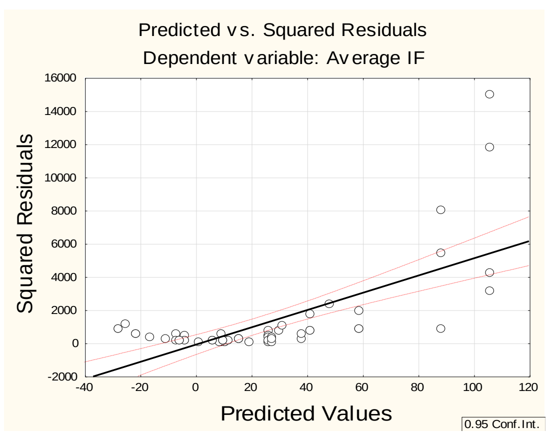

(c)

Fig. 24 Performance of Eq. (7) for IF_{ave} by STATISTICA

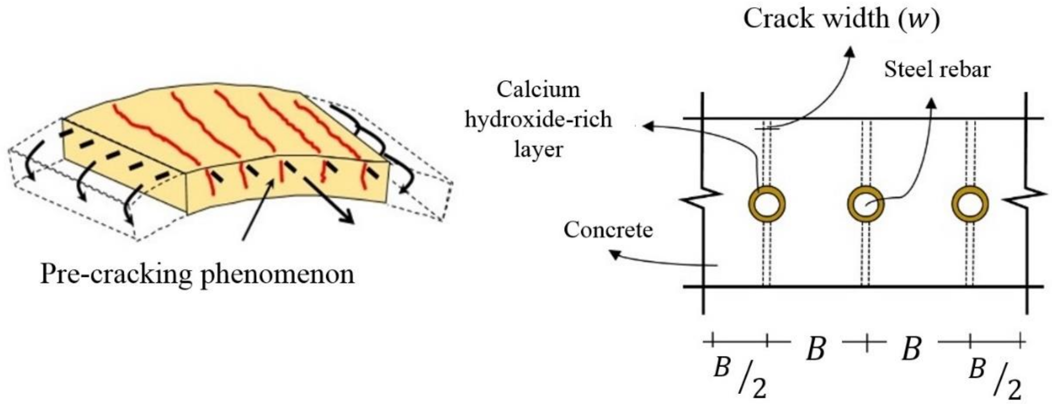

(a)

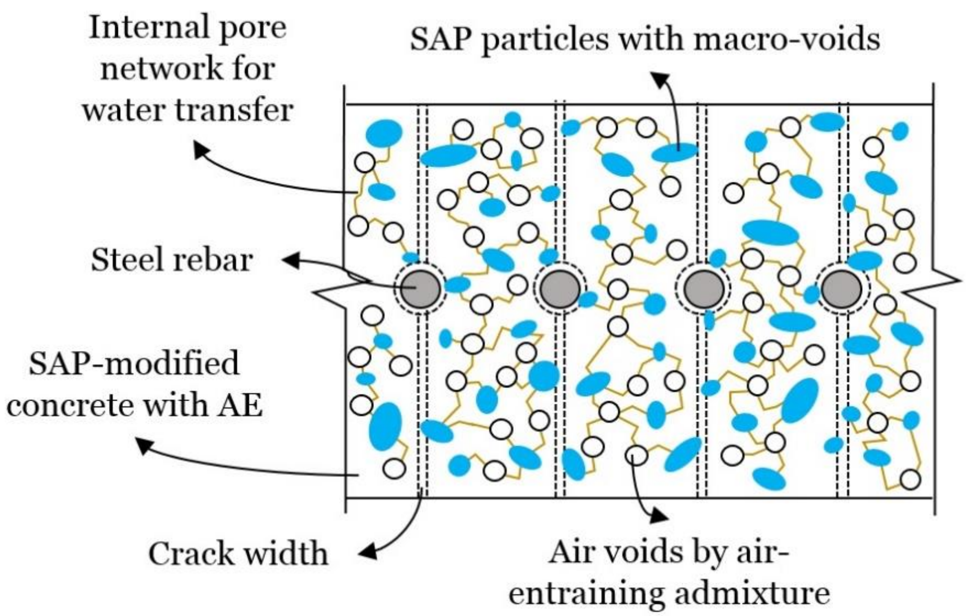

(b)

Fig. 25 Schematic representation of the Buffon needle problem: (a) existence of Ca(OH)2 around rebar for increasing the probability of crack healing; (b) internal pore network for water transfer in self-healing method of SAP concrete containing AE admixture

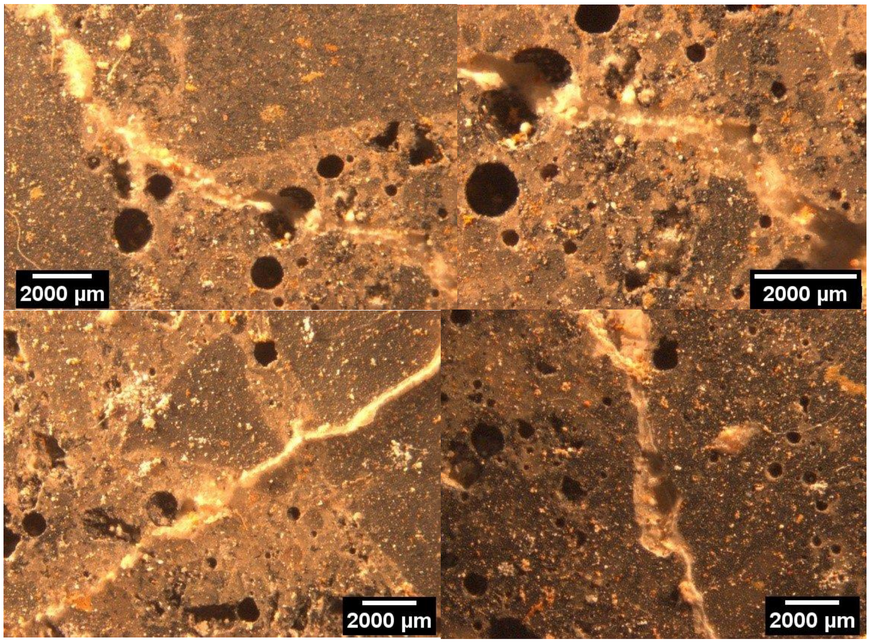

Fig. 26 Distribution of SAP and AE pores around the crack path (1.00SAP1AE-healed)